iScience

CellPress
OPEN ACCESS

Article

Design, synthesis, and physicochemical study of a biomass-derived CO_2 sorbent 2,5-furan-bis(iminoguanidine)

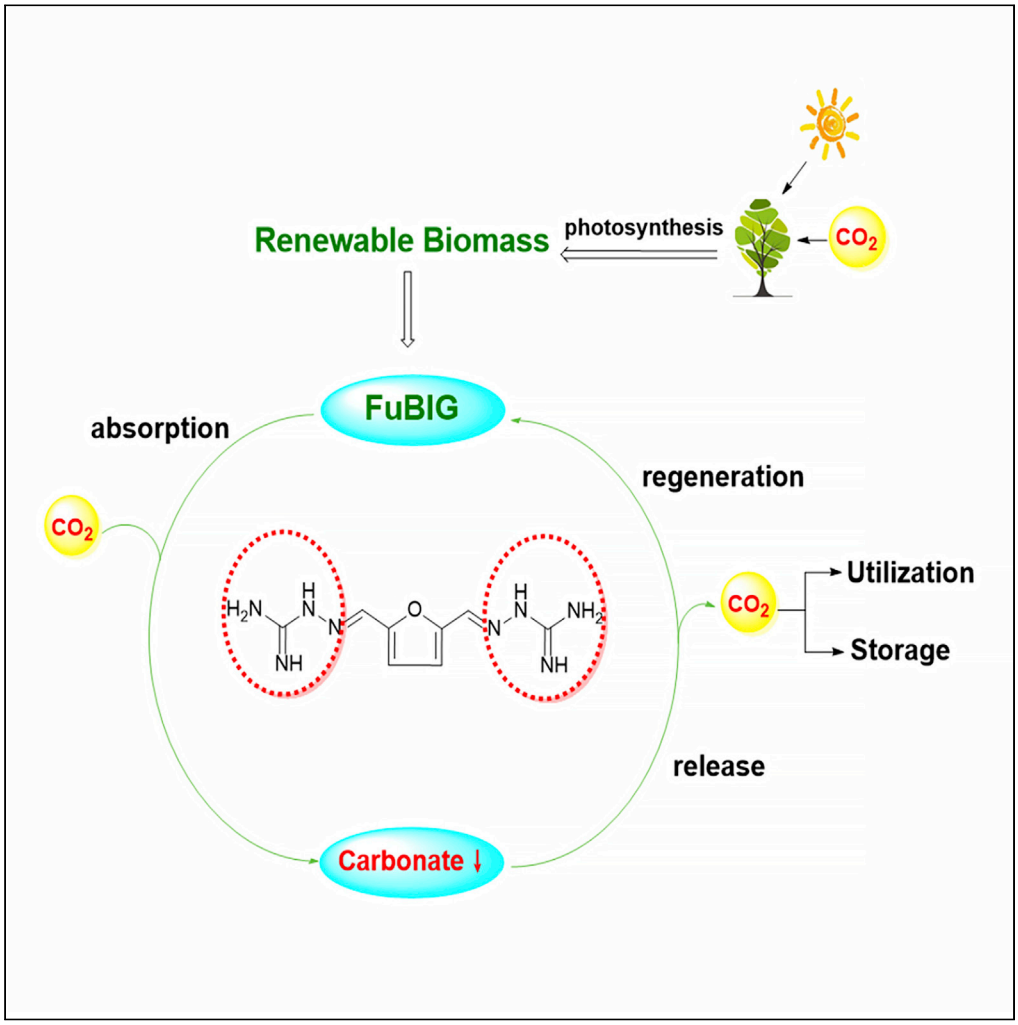

Qianzhong Zhang, Yi Jiang, Yinwu Li, Xianheng Song, Xiang Luo, Zhuofeng Ke, Yong Zou

zouyong3@mail.sysu.edu.cn

Highlights

The concept of biomass-derived direct air capture has been proposed and reinforced by the sorbent of FuBIG

The sorbent revealed favorable thermodynamic and kinetic parameters for CO_2 capture and release

The sorbent has excellent biocompatibility and good thermostability

FuBIG carbonate can release CO_2 and regenerate FuBIG spontaneously in DMSO without heating

Zhang et al., iScience 24, 102263
April 23, 2021
https://doi.org/10.1016/j.isci.2021.102263

iScience

CellPress
OPEN ACCESS

Article

Design, synthesis, and physicochemical study of a biomass-derived CO_2 sorbent 2,5-furan-bis(iminoguanidine)

Qianzhong Zhang,[1] Yi Jiang,[1] Yinwu Li,[2] Xianheng Song,[1] Xiang Luo,[1] Zhuofeng Ke,[2] and Yong Zou[1,3,4,*]

SUMMARY

In this study, the concept of biomass-based direct air capture is proposed, and the aminoguanidine CO_2 chemical sorbent 2,5-furan-bis(iminoguanidine) (FuBIG) was designed, synthesized, and elucidated for the physicochemical properties in the process of CO_2 capture and release. Results showed that the aqueous solution of FuBIG could readily capture CO_2 from ambient air and provided an insoluble tetrahydrated carbonate salt $FuBIGH_2(CO_3)(H_2O)_4$ with a second order kinetics. Hydrogen binding modes of iminoguanidine cations with carbonate ions and water were identified by single-crystal X-ray diffraction analysis. Equilibrium constant (K) and the enthalpies (ΔH) for CO_2 absorption/release were obtained by thermodynamic and kinetic analysis ($K_7 = 5.97 \times 10^4$, $\Delta H_7 = -116.1$ kJ/mol, $\Delta H_8 = 209.31$ kJ/mol), and the CO_2-release process was conformed to the geometrical phase-boundary model $(1-(1-\alpha)^{1/3} = kt)$. It was found that the $FuBIGH_2(CO_3)(H_2O)_4$ can release CO_2 spontaneously in DMSO without heating. Zebrafish models revealed a favorable biocompatibility of FuBIG.

INTRODUCTION

The heavy reliance and massive consumption of fossil resources in modern society has caused continuous rising of atmospheric CO_2 concentration and resulted in an alarming change of global climate (Cox et al., 2020; Davis et al., 2018; Anderson et al., 2018; Jin et al., 2020). Carbon capture and storage (CCS) has been proposed and implemented as a feasible strategy to reduce the point-source CO_2 emissions (Lackner, 2003; Reiner, 2016; Burant et al., 2017; Zhai et al., 2015; Sha et al., 2016; Bui et al., 2018; Wang, 2016). However, as the dispersed CO_2 emissions account for 50% of total greenhouse emissions (Seipp et al., 2017), the application of point-source CCS technologies is unlikely to stabilize the atmospheric CO_2 concentration at a desirable level (Sanz-Pérez et al., 2016). Accordingly, the concept of direct air capture (DAC) has been put forward which aims at capturing CO_2 from ambient air (National Research Council, 2015; Keith, 2009; Sutherland, 2019; Jacobson, 2019; Bajamundia et al., 2019; Shi et al., 2020). In the past two decades, many efforts have been devoted for the development of various DAC sorbents, such as porous organic polymers (POPs), metal-organic frameworks (MOFs), solid-supported amine-based sorbents, and small molecular organic sorbents. Among them, the POPs are polymeric materials constructed by organic covalent bonds which are considered to be promising materials for CO_2 storage due to the hyper-crosslinked structures and high stability (Zou et al., 2017; Li et al., 2017; Wang et al., 2017; Yang et al., 2019). The MOFs are highly porous materials constructed by metal cations and organic ligands which have large surface areas and can effectively trap carbon dioxide in the cages (Boyd et al., 2019; Trickett et al., 2017; González-Zamora and Ibarra, 2017). Solid-supported amine-based sorbents are solid adsorbents which incorporate amine moieties into solid supports including zeolites, carbons and organic resins, etc (Thakkar et al., 2017; Pang et al., 2017; Holewinski et al., 2017; Sarazen and Jones, 2017). These adsorbents offer advantages such as high selectivity for CO_2 and relatively low cost, but they displayed lower CO_2 capacities compared to other sorbents. In recent years, some specially designed organic compounds have shown great potential for DAC. For example, in 2014, Hossain group developed an organic compound with six urea groups which absorbed atmospheric CO_2 as CO_3^{2-} via 12 strong N—H•••O bonds under mild conditions (Pramanik et al., 2014). In 2017, Custelcean et al. reported an innovative iminoguanidine type sorbent, namely 2,6-pyridine-bis(iminoguanidine) (PyBIG) which could capture CO_2 from ambient air, crystallize as an insoluble carbonate and regenerate PyBIG by mild heating with concomitant CO_2 releasing (Seipp et al.,

[1]School of Pharmaceutical Sciences, Sun Yat-sen University, Guangzhou 510000, P. R. China

[2]School of Chemistry, Sun Yat-sen University, Guangzhou 510000, P. R. China

[3]Guangdong Provincial Key Laboratory of Chiral Molecule and Drug Discovery, Guangzhou 510000, P. R. China

[4]Lead contact

*Correspondence: zouyong3@mail.sysu.edu.cn

https://doi.org/10.1016/j.isci.2021.102263

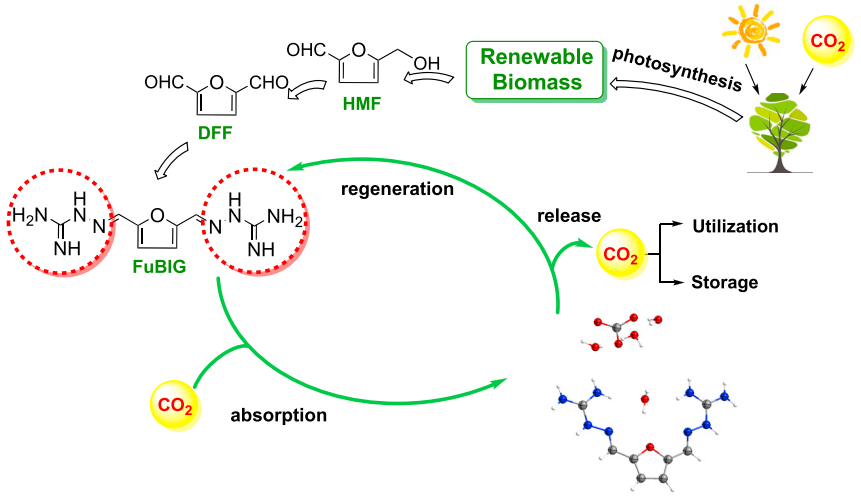

Figure 1. Illustration of the design, synthesis of the biomass-derived sorbent FuBIG showing negative emission properties following the concept of BBDAC

2017; Brethomé et al., 2018). Soon after, they disclosed another simple and robust iminoguanidine compound called glyoxal-bis(iminoguanidine) (GBIG), by which the flue gas CO_2 absorption led to the formation of a dehydrated bicarbonate salt (Williams et al., 2019; Garrabrant et al., 2019); however, further results proved that the GBIG was ineffective for DAC (Custelcean et al., 2020). In addition, their most recent structure-property relationship study of GBIG, MGBIG (methylglyoxal-bis(iminoguanidine)) and DABIG (diacetyl-bis(iminoguanidine)) revealed that minor modifications in the molecular structures would result in dramatic differences in the crystal structures, aqueous solubilities, conformational flexibilities, as well as free energies for CO_2 absorption (Custelcean et al., 2020). Although great progress has been made, the development of DAC sorbents for CO_2 capture is still in its infancy. Thus, strategies and solutions for DAC processes that are facile, efficient, economical, independent of fossil resources, and applicable on a large scale would be highly desired.

From the viewpoints of green chemistry and climate change, the chemical conversion and utilization of biomass represent a kind of carbon neutral processes which would be more eco-friendly compare with the utilization of fossil resources (Chheda et al., 2007; Ji et al., 2018; Strube et al., 2011). As an indirect source of solar energy, biomass is abundant and renewable in nature. It is generally accepted that large-scale and efficient utilization of biomass would cause no net increase of carbon and would exert beneficial effects against global warming (Chheda et al., 2007; He et al., 2019; Ma et al., 2011).

Platform molecules are recognized as vital hallmarks of biomass conversion and utilization which can be utilized as starting materials or building blocks for the production of a great number of downstream chemicals (Serrano-Ruiz et al., 2011; Arias et al., 2020; Luterbacher et al., 2014; Zhu et al., 2017). Among them, the 5-hydroxymethylfurfural (5-HMF) is one of the most versatile and highly transformable bio-based platform molecules originated from lignocellulose (Ma et al., 2011; Zhu et al., 2017; Saha and Omar, 2014; Solanki and Rode, 2019; Zhao et al., 2007). The partial oxidized derivative of 5-HMF, namely, 2,5-diformylfuran (DFF) has also been widely used as a starting material for the synthesis of pharmaceuticals, macrocyclic ligands, and functional polymeric materials (Ghatta et al., 2019; Zhang and Huber, 2018; Zhao et al., 2018). Inspired by the concept of bioenergy with carbon capture and storage (BECCS) (Davis et al., 2018), and as part of our continuing efforts on biomass conversion and utilization (Wu et al., 2012; Luo et al., 2019; Huang et al., 2018; Sheng et al., 2016; Zhang et al., 2014a, 2014b, 2014c, 2015), we envisioned that the concept of biomass conversion and DAC could be combined to the description of biomass-based direct air capture (BBDAC, Figure 1.). More specifically, we envisaged that the development of an iminoguanidine type of CO_2 sorbents based on biomass-derived platform molecules would be rational and more favorable to achieve the goal of negative emissions. Herein, we report the design, synthesis, physicochemical study, and swing property of an efficient CO_2 sorbent, the 2,5-furan-bis(iminoguanidine) (FuBIG), starting from the biomass-derived DFF.

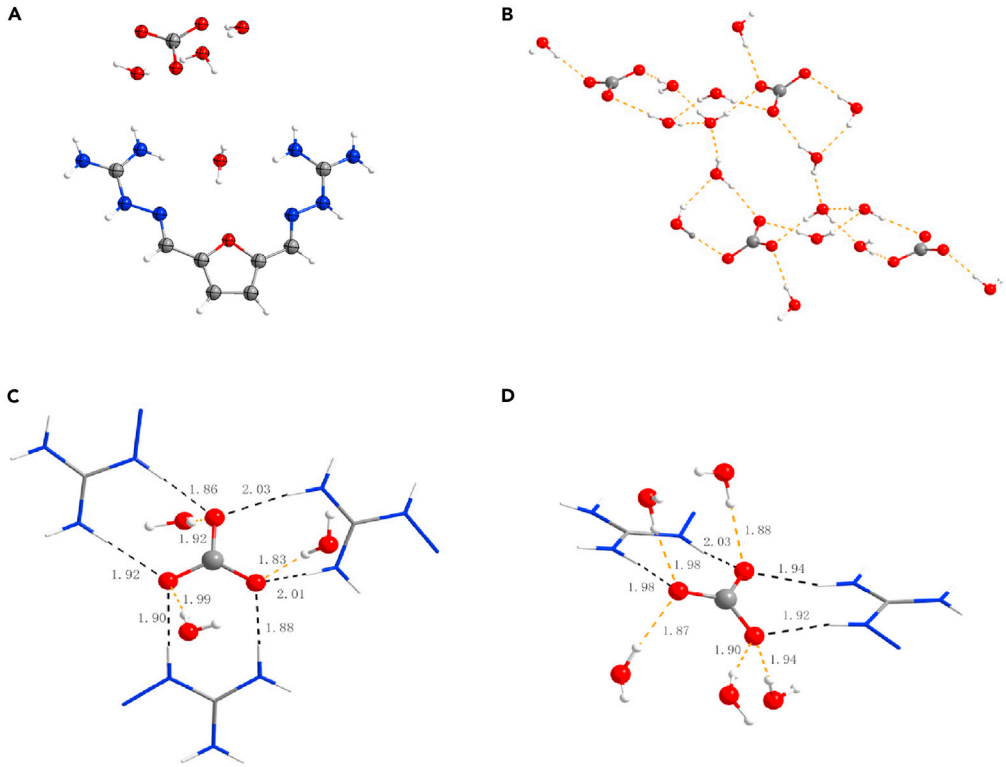

Figure 2. Atmospheric CO_2 capture by FuBIG lead to the crystallization of $FuBIGH_2(CO_3)(H_2O)_4$ and the X-Ray crystal structure analysis

(A) X-ray single crystal structure of $FuBIGH_2(CO_3)(H_2O)_4$ with 50% ellipsoids. (C, gray; H, white; N, blue; O, red.).

(B) Ladder-shaped hydrogen-bonded $[(CO_3)(H_2O)_4]_n$ anionic cluster.

(C) Binding mode A: each carbonate anion in the cluster accepted three water hydrogen bonds and six guanidinium hydrogen bonds. The $FuBIGH_2^{2+}$ cations have been truncated at the imine bond.

(D) Binding mode (B): each carbonate anion in the cluster accepted five water hydrogen bonds and four guanidinium hydrogen bonds.

RESULTS AND DISCUSSION

Synthesis, physical properties and crystallization analysis of FuBIG

The FuBIG was readily obtained by the imine condensation of the biomass-derived DFF with aminoguanidinium chloride, followed by neutralization with aqueous NaOH. Gratifyingly, the FuBIG showed an improved aqueous solubility (0.4029 M, 25°C) than PyBIG (0.0012 M, 25°C), and when the aqueous solution of FuBIG was left open to ambient air for a few days, the formation of prism shaped, yellowish-brown single crystals was found, which was consistent with the composition of a tetrahydrated carbonate $FuBIGH_2(CO_3)(H_2O)_4$ by Fourier transform infrared spectroscopy (FTIR), elemental analysis (EA), and single-crystal X-ray diffraction analysis (CCDC: 2038310, Table S1, Figures S8 and 2A). Moreover, results showed that the ladder-shaped $[(CO_3^{2-})(H_2O)_4]_n$ anionic cluster was formed and extended through hydrogen-bonds (Figure 2B). Interestingly, it was found that there were a total of nine hydrogen bonds with two types of binding modes (A and B) existing in every two adjacent carbonate anion in the crystal structures of $FuBIGH_2(CO_3)(H_2O)_4$. In binding mode A (Figure 2C), each carbonate anion in the cluster accepted three water hydrogen bonds to form $[CO_3(H_2O)_4^{2-}]_n$ clusters, with O—H•••O contact distances ranging between 1.83 and 1.99 Å, and with bond angles between 170° and 172°. Furthermore, each carbonate anion also accepted another six guanidinium hydrogen bonds, with N—H•••O contact distances ranging between 1.88 and 2.03 Å, and bond angles between 157° and 176°. In binding mode B (Figure 2D), the carbonate anion accepted five hydrogen bonds from water with O—H•••O contact distances ranging between 1.87 and 1.98 Å, and with bond angles between 166° and 177°. Correspondingly, the carbonate anion accepted another four guanidinium hydrogen bonds, with N—H•••O contact distances ranging between 1.92 and 2.03 Å, and with bond angles between 157° and 168°. Single-crystal X-ray diffraction analysis of $FuBIGH_2(CO_3)(H_2O)_4$ displayed that the hydrogen bonding between FuBIG, CO_2 (as CO_3^{2-}), and H_2O

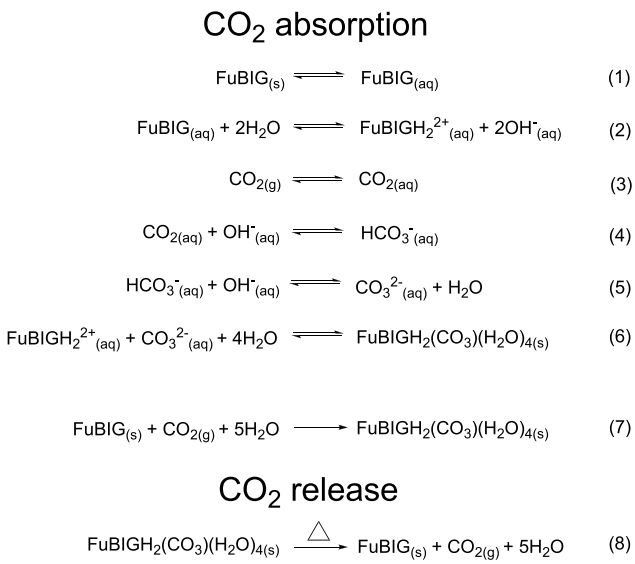

Scheme 1. Stepwise and overall reactions in CO_2 capture process of FuBIG and CO_2 heat release of its carbonate salt

was significant and would be the main driving force for the capture of CO_2 in ambient air. Moreover, the energy of the hydrogen bonds has been analyzed by DFT study. The energy of the hydrogen bonds between $FuBIGH_2^{2+}$ and CO_3^{2-} is calculated to be 16.4 kcal/mol, and the energy of the hydrogen bonds between $FuBIGH_2(CO_3)$ and H_2O is calculated to be 6.5 kcal/mol (see Table S12: The cartesian coordinates (xyz) for hydrogen bonds on DFT calculation for details). These results suggest that hydrogen bonds would provide a delicate balance between the stability of $FuBIGH_2(CO_3)(H_2O)_4$ and the property of FuBIG regeneration and CO_2 release.

Thermodynamic and kinetic analysis of CO_2 absorption and heat release

The thermodynamic and kinetic study of CO_2 absorption and heat release are crucial tasks in the search for CO_2 sorbents, which could provide accurate physicochemical parameters and minimum energy requirements for the reactions in stepwise and overall manner, thereby paving the way for further optimization and application. The reactions involved in the CO_2 absorption and heat release regarding FuBIG are shown in Scheme 1, and the corresponding thermodynamic parameters are listed in Table 1.

The reactions involved in the CO_2 absorption comprise six steps represented by Equations (1)–(6) in Scheme 1. First, FuBIG dissolves into water (Equation 1), followed by acceptance of two protons from water to generate the $FuBIGH_2^{2+}$ cations and OH^- (Equation 2). Then, CO_2 transports from air into aqueous solution (Equation 3) and reacts with OH^- to generate HCO_3^- (Equation 4) and subsequently give CO_3^{2-} (Equation 5). Finally, the $FuBIGH_2^{2+}$ and CO_3^{2-} ions crystallize with water to afford $FuBIGH_2(CO_3)$ $(H_2O)_4$ (Equation 6).

The corresponding enthalpy (ΔH) values for Equations (1)–(6) are listed in Table 1, the enthalpies of CO_2 dissolution (Equation 3, $\Delta H_3 = -19.4$ kJ/mol), and the generation of HCO_3^- and CO_3^{2-} (Equations 4 and 5, $\Delta H_4 = -50$ kJ/mol, $\Delta H_5 = -40.4$ kJ/mol) were obtained from previous studies (Carroll et al., 1991; Wang et al., 2010; McCann et al., 2011). The remaining enthalpies for the reactions including FuBIG dissolution (Equation 1) and $FuBIGH_2(CO_3)$ $(H_2O)_4$ crystallization (Equation 6) were determined by van't Hoff analysis of variable temperature solubility assay, respectively ($\Delta H_1 = -49.19$ kJ/mol, $\Delta H_6 = -101.57$ kJ/mol, Figures S11 and S12, Tables S4 and S5). Similarly, the enthalpy for FuBIG protonation (Equation 2) were obtained from van't Hoff analysis of variable temperature pK_a assay ($\Delta H_2 = -46.08$ kJ/mol Table S7 and Figure S13). The overall reaction of CO_2 absorption is represented by Equation 7 (Scheme 1), which has an overall enthalpy (ΔH_7) of −116.10 kJ/mol. These results showed that the overall enthalpy value was more negative from FuBIG to $FuBIGH_2(CO_3)$ $(H_2O)_4$ than that from PyBIG to

Table 1. Thermodynamic and kinetic parameters for CO_2 capture and heat release

Entry	Reaction/parameter	ΔH (kJ/mol)[c]	K[c]	Solubility (mol/L)[c]	Reference
1	FuBIG dissolution	$\Delta H_1 = 49.19$[d]	$K_1 = 4.03 \times 10^{-1}$ [i]	$S_1 = 0.4029$	Figure S10
2	FuBIG protonation[a]	$\Delta H_2 = 46.08$[e]	$K_2 = 1.91 \times 10^{-12}$ [j]	–	Figure S12
3	CO_2 dissolution	$\Delta H_3 = -19.4$	$K_3 = 3.4 \times 10^{-2}$	–	Carroll et al., 1991
4	HCO_3^- formation	$\Delta H_4 = -50$	$K_4 = 3.02\times10^{7}$	–	Wang et al., 2010
5	CO_3^{2-} formation	$\Delta H_5 = -40.4$	$K_5 = 4.66\times10^{3}$	–	McCann et al., 2011
6	$FuBIGH_2(CO_3)(H_2O)_4$ crystallization	$\Delta H_6 = -101.57$[f]	$K_6 = 1.63\times10^{7}$ [k]	$S_6 = 0.009344$	Figure S11
7	overall CO_2 absorption	$\Delta H_7 = -116.1$[g]	$K_7 = 5.97 \times 10^{4}$[l]	–	Table 1
8	CO_2 release[b]	$\Delta H_8 = 209.31$[h]	–	–	Figure S15
9	$[R_s]$	–	–	43.12[m]	Figures S10 and S11

[a]This reaction included a double deprotonation processes of water.
[b]CO_2 heat release was measured at a persistent heating rate (10°C/min).
[c]The parameters were determined at standard temperature (25°C) unless otherwise specified.
[d]Determined by van't Hoff analysis of solubility values of FuBIG measured in the 15–35°C range.
[e]The enthalpies for the protonation processes of FuBIG were calculated by van't Hoff analysis of pK_a values measured in the 15–35°C range, and included the enthalpies for a double deprotonation processes of water (55.8 kJ/mol).
[f]Determined by van't Hoff analysis of K_{sp} values measured in the 15–35°C range.
[g]$\Delta H_7 = \Delta H_1 + \Delta H_2 + \Delta H_3 + \Delta H_4 + \Delta H_5 + \Delta H_6$.
[h]Determined from the endotherm observed in the DSC.
[i]$K_1 = K_{sp}$(FuBIG).
[j]$K_2 = (K_w)^2/(K_{a1} \times K_{a2})$.
[k]$K_6 = 1/K_{sp}(FuBIGH_2(CO_3)(H_2O)_4)$.
[l]$K_7 = K_1\times K_2\times K_3\times K_4\times K_5\times K_6$.
[m]$[R_s] = S_1/S_6$.

$PyBIGH_2(CO_3)(H_2O)_4$ (−70.7 kJ/mol) (Brethomé et al., 2018), indicating that the CO_2 absorption of FuBIG was more exothermic and would be easier to take place than that of PyBIG.

The overall equilibrium constant for CO_2 absorption is 5.97×10^4 ($K_7 = K_1\times K_2\times K_3\times K_4\times K_5\times K_6$, Table 1). It is worth-mentioning that the values of K_3, K_4 and K_5 are invariable under ideal conditions, so the extent of the overall reaction of any specially designed aminoguanidine sorbent could be improved with the increase of basicity (K_2) and solubility of the free base (K_1) and the decrease of solubility of its carbonate salt (K_6). Specifically, strong basicity of the sorbent would facilitate the transformation of CO_2 to CO_3^{2-}, high solubility of the free base would make the aqueous solution of the sorbent to interact with the gaseous CO_2 more efficiently, whereas the low solubility of the corresponding carbonate salt would lead to the precipitation more thorough and the separation of which by filtration more convenient. However, as the differences of basicity between iminoguanidine sorbents are generally indistinctive, therefore, the solubility of the free base and its carbonate salt would be the simple and determining factors for this kind of sorbents. Accordingly, The value $[R_s]$ was introduced in this study which was defined as the solubility ratio between FuBIG and its carbonate $FuBIGH_2(CO_3)(H_2O)_4$ at 25°C ($[R_s] = 43.12$, Table 1, Tables S4 and S5). Moreover, according to solubility data reported by Custelcean et al. (Brethomé et al., 2018; Williams et al., 2019), the $[R_s]$ value for PyBIG and GBIG were determined to be 7.97 and 1.60, respectively. Thus, the results suggested that the FuBIG would be more favorable as a CO_2 sorbent than PyBIG and GBIG in terms of $[R_s]$ value.

When the crystals of $FuBIGH_2(CO_3)(H_2O)_4$ were heated in an oven at 120°C for 1h, the crystals transformed to FuBIG and changed their appearance from transparent to opaque, while maintaining the original yellow color (Figure S15). Thermogravimetric analysis (TGA) provided a quantitative measurement of the decomposition process (Figure 3A). $FuBIGH_2(CO_3)(H_2O)_4$ showed a 35.71% mass loss between 72°C and 148°C, which was consistent with the loss of 1 equiv. of carbonic acid (as CO_2 and H_2O) and 4 equiv. of H_2O (36.22% theoretical mass loss). After the complete regeneration of FuBIG at 148°C, the TGA curve became flat with the increase of temperature to about 220°C, this result indicated that there was no thermal decomposition occurred in this temperature range, demonstrating a high thermostability of FuBIG. Subsequently, it was found that the FuBIG began to decompose at around 240°C with further increment of temperature. In addition, the very similar TGA pattern between $FuBIGH_2(CO_3)(H_2O)_4$ and FuBIG at above 140°C, fully confirmed the regeneration process

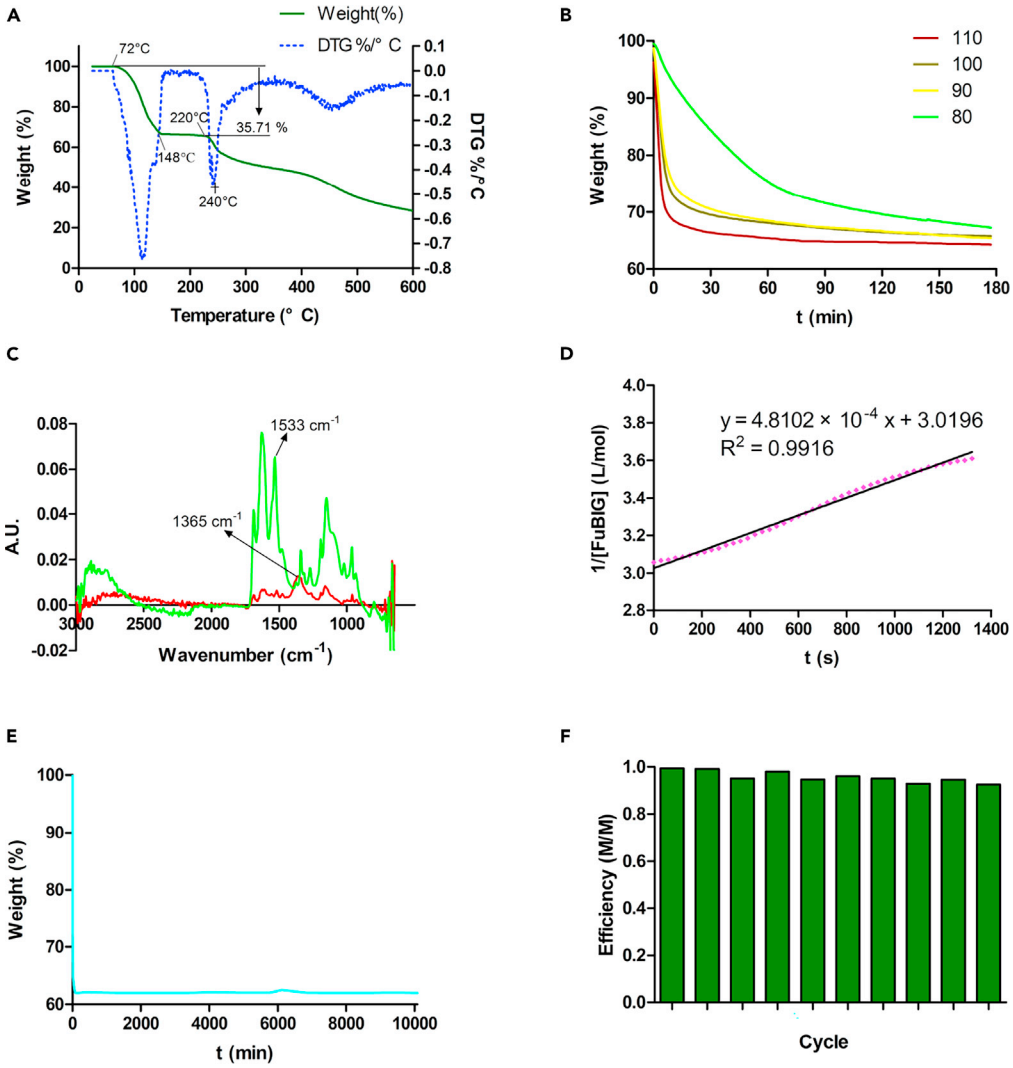

Figure 3. Thermodynamic and kinetic analysis of CO_2 absorption and release with FuBIG and applicability evaluation in practical process

(A) Temperature-ramped TGA plots showing CO_2 and H_2O release from $FuBIGH_2(CO_3)(H_2O)_4$.

(B) Isothermal TGA data used for the kinetic analysis of CO_2 release from $FuBIGH_2(CO_3)(H_2O)_4$ at 80°C, 90°C, 100°C, 110°C.

(C) Infrared absorption of FuBIG (green) and its carbonate (red), the peak at 1533 cm^{-1} is the characteristic N-H absorption of FuBIG, while the peak at 1365 cm^{-1} representing the wavenumber of the carbonate salt.

(D) The simulated pattern of reaction order for CO_2 absorption with FuBIG at 25°C.

(E) Isothermal (110°C) thermogravimetric analysis of $FuBIGH_2(CO_3)(H_2O)_4$ in air over a one-week period.

(F) Efficiency of CO_2 sorbent (M/M) over ten consecutive absorption-release cycles.

from $FuBIGH_2(CO_3)(H_2O)_4$ to FuBIG under thermal conditions (Figures 3A and S14). Overall, the CO_2 capture of the biomass-based FuBIG from ambient air and heat release of CO_2 with concomitant regeneration of the sorbent provided direct experimental evidence for the feasibility of BBDAC.

The differential scanning calorimetry (DSC) analysis of $FuBIGH_2(CO_3)(H_2O)_4$ displayed an endothermic pattern corresponding to the loss of CO_2 and H_2O in TGA study, with a measured releasing enthalpy (ΔH_8) of 209.31 kJ/mol (Figure S16). Before the temperature reached the point for CO_2 release, it could be calculated from the DSC measurements that an enthalpy of 48.40 kJ/mol was needed for the specific heat capacity of $FuBIGH_2(CO_3)(H_2O)_4$ (Figure S17). Hence, the total enthalpy requirement for the regeneration of FuBIG would be 257.71 kJ/mol.

Isothermal TGA running at constant temperatures of 40, 50, 60, 70, 80, 90, 100, and 110°C respectively, provide evidence for the kinetic analysis of the CO_2 and H_2O released from $FuBIGH_2(CO_3)(H_2O)_4$ (Figure S18). Among them, it was found that the practical and effective data was obtained from temperature range of 80, 90, 100, and 110°C (Figure 3B). After plotting the fractional conversion (α) as a function of time (Figure S19), the most common solid-state reaction kinetics, including Avrami-Erofeev, Prout-Tompkins, Ginstling-Brounstein, Jander, and geometrical phase-boundary models were screened (Figure S20). It was found that the most fitted model would be assigned to the geometrical phase-boundary model characterized by Equation (9):

$$1-(1-\alpha)^{1/3}=kt,\ \alpha=(m_0-m)/(m_0-m_f) \quad \text{(Equation 9)}$$

Where m_0 represents the initial sample weight of FuBIG carbonate salt, m_f represents the final weight after isothermal heating, and m represents the sample weight at a certain time (Figure S20). This result revealed that the reaction initiated on the surface of crystals, followed by inward advance to the center, and resulting in a decelerator α-t curve with the decrease of interface. Moreover, activation barrier (E_a = 92.24 kJ/mol) for the decomposition of $FuBIGH_2(CO_3)(H_2O)_4$ was obtained from Arrhenius analysis of the rate constants (k) under different temperatures (Figure S21).

The recycling kinetics of CO_2 absorption and release corresponding to the transformation of FuBIG—$FuBIGH_2(CO_3)(H_2O)_4$—FuBIG could be characterized by *in situ* React IR in solution state. The characteristic wavelength of FuBIG and $FuBIGH_2(CO_3)(H_2O)_4$ were found to be 1533 cm^{-1} (N—H) and 1365 cm^{-1} (CO_3^{2-}), respectively (Figure 3C). By monitoring the intensity change of these absorption peaks, the corresponding concentration changes of FuBIG and FuBIG carbonate salt could be obtained. As shown in Figure S23, when CO_2 was put into the aqueous solution of FuBIG, the concentration of FuBIG decreased with the formation of FuBIG carbonate salt (the concentration change of carbonate anion was relatively complicated owing to the multifactorial influence toward the labile FuBIG carbonate salt under thermal conditions in solution state). By analyzing the concentration-time curve of FuBIG with integral method, it could be found that the process of CO_2 absorption was in accordance with the second order reaction kinetics with a rate constant (k) of 4.8102 × 10^{-4} L/mol·s at 25°C (Figure 3D).

Applicability evaluation of FuBIG in practical process

It is widely accepted that the recycling of both CO_2 and the sorbent is indispensable in practical CCUS process (Gao et al., 2020; Flores-Granobles and Saeys, 2020; Leclaire and Heldebrant, 2018; Gonzalez-Diaz et al., 2020). Therefore, in this study, the crystals of $FuBIGH_2(CO_3)(H_2O)_4$ were heated at 110°C in oven for one week for the investigation of the robustness of FuBIG in CO_2 capturing and releasing process. The weight was measured every 6 hr. After the release of CO_2 and H_2O, FuBIG showed no sign of decomposition (Figure 3E). The weight of the solid was fluctuating within a narrow range.

Next, we ran a full CO_2 separation cycle using CO_2 balloon to assess the recyclability of this sorbent. CO_2 gas was injected into the saturated aqueous solution of FuBIG, leading to the formation of yellow precipitate within minutes. The solid was collected by filtration and the filtrate was analyzed by ultraviolet-visible spectroscopy to determine the concentration of the free FuBIG left in the solution. At the first cycle, 99.36% of FuBIG was converted to the FuBIG carbonate salt. Then the FuBIG carbonate salt was heated at 110°C for 4h, leading to complete release of CO_2 and H_2O. The regenerative FuBIG was then dissolved into the filtrate and precipitated again by CO_2. Overall, ten consecutive CO_2 capture/release cycles were conducted, and the conversion rate could still maintain at 92.49% (Figure 3F). Although the long-term stability and recyclability of FuBIG remains to be explored over more and more capture/release cycles under practical conditions, our preliminary results indicated that this biomass-derived sorbent is remarkably robust.

The transformation of CO_2 into bulk chemicals or value-added products represents an attractive strategy for CO_2 utilization. In our previous work, a facile and operationally simple method (room temperature, 1 atm of CO_2 balloon) for the synthesis of various *O*-aryl carbamates via one-pot three-component coupling of aryl carboxamides, CO_2, and amines has been established (Luo et al., 2019). We reasoned that the CO_2 captured by biomass-derived sorbent FuBIG could be utilized in chemical reactions. Accordingly, in this study, a round bottom flask filled with $FuBIGH_2(CO_3)(H_2O)_4$ in place of CO_2 balloon was connected with the reaction system, the CO_2 airflow was stably generated at 80°C, and reacted with aryl carboxamide and amine to afford the desired *O*-aryl carbamate in 70% yield in the presence of CuI and MnO_2 (Figure S24)

(Luo et al., 2019). This result demonstrated the feasibility for the circulation of CO_2 capture, release and utilization regarding the transformation between FuBIG and FuBIG carbonate salt and represented a practical example for negative emissions under the proposed BBDAC rationale.

Spontaneous CO_2 release of FuBIG carbonate salt in DMSO

The regeneration convenience and long-term robustness of CO_2 sorbents are vital factors in the development of practical and efficient DAC technologies. It is quite obvious that, for an optimal CO_2 sorbent, large energy requirement should be avoided for CO_2 release and sorbent regeneration. However, to the best of our knowledge, current DAC technologies including humidity swing, pressure swing, or temperature swing, are energy-intensive, strongly endothermic and complicated in the operating processes. Surprisingly and delightfully, during the recording of the NMR spectra for FuBIG carbonate salt, some interesting results displaying a unique, unprecedented, and spontaneous way for CO_2 release from FuBIG carbonate salt were obtained. It was found that when DMSO-d_6 was added into the FuBIG carbonate salt with oscillation at room temperature, the insoluble solid gradually dissolved with concomitant release of CO_2 in an endothermic manner in a few minutes. The ^{1}HNMR and ^{13}CNMR spectra gave identical results compared with that of FuBIG, demonstrating a unique and easy way for CO_2 release and regeneration of FuBIG from its carbonate salt in DMSO-d_6 (Figures S4 and S5). Subsequently, the non-deuterated DMSO was tested (showed by React IR in Figure 4A), and the same result was obtained. Amazingly, other commonly used solvents such as tetrahydrofuran, ethanol, methanol, ethyl acetate, and chloroform etc. were unable to regenerate FuBIG from its carbonate salt under the same conditions. Our findings regarding the spontaneous CO_2 release of FuBIG carbonate salt in DMSO/DMSO-d_6 might represent a technique with near-zero energy input and might open up a new avenue for DAC technologies.

To gain further insight into the spontaneous process for CO_2 release of FuBIG carbonate salt in DMSO, calculation studies were carried out by density functional theory (Hohenberg and Kohn, 1964; Kohn and Sham, 1965). As illustrated in Figures 4B and 4C, owing to the existence of hydrogen bonds, the binding energy representing by ΔH and ΔG between H_2CO_3 and FuBIG are more negative in value than that of between DMSO and FuBIG (for interaction of H_2CO_3 with FuBIG: $\Delta H/\Delta G = -26.7/-2.5$ kcal/mol; for interaction of DMSO with FuBIG: $\Delta H/\Delta G = -10.9/10.3$ kcal/mol). Therefore, the extrusion of CO_2 from FuBIG carbonate salt in DMSO should not result from stronger interaction between DMSO and FuBIG. Moreover, as shown in Figure 4D, the reaction between H_2CO_3 and FuBIG in water to form FuBIG carbonate salt is spontaneous ($\Delta G = -1.5$ kcal/mol), whereas the same reaction taken place in DMSO is nonspontaneous ($\Delta G =$ 35.5 kcal/mol) (see Table S13: The cartesian coordinates (xyz) for all optimized structures on DFT calculation for details). Accordingly, it could be concluded that H_2CO_3 and FuBIG are more in inclined to form the ion pair ($FuBIGH_2^{2+} \cdot CO_3^{2-}$) in water, while the counterreaction of which is more likely to take place in DMSO.

Interestingly, we have also found that the DMSO solution saturated with FuBIG could still promote the release of CO_2 from FuBIG carbonate, and result in the regeneration of FuBIG. This intriguing result indicated that a dynamic equilibrium might be achieved for CO_2 release and FuBIG regeneration in these conditions, thereby providing a proof of concept for a highly efficient and energy-saving protocol for the cycling of CO_2 capture, release and sorbent regeneration. It is obvious that under these conditions, the recovery of FuBIG (by filtration) from DMSO could be realized spontaneously and continuously with minimum DMSO consumption, and evaporation of DMSO is no longer needed for the sorbent recovery (Figures S25 and S26). In addition, freeze drying might be another option for DMSO removing and sorbent recovery.

Biocompatibility assay of FuBIG

The future application scenarios of DAC sorbents could be classified into two categories: exceptionally large-scale deployments for CO_2 capture either from point-sources or from ambient atmosphere, and small-scale facilities for CO_2 capture in enclosed cabins such as space capsules or submarines. Accordingly, the biocompatibility properties of DAC sorbents should be taken into consideration. In this study, zebrafish were used as the model species, the tests of acute toxicity and embryo toxicity were conducted, respectively, for the biocompatibility evaluation of FuBIG and the previously reported PyBIG. Results showed that the FuBIG was less toxic than PyBIG in acute toxicity test in terms of maximum non-lethal concentration (MNLC) and 10% lethal concentration (LC_{10}), with the corresponding measurements for FuBIG (MNLC = 39.6 μM, LC_{10} = 54 μM) and PyBIG (MNLC = 17.1 μM, LC_{10} = 24 μM), respectively (Figures 5A and 5B). In target organ toxicity tests of FuBIG (1.9, 5.7, 17.1, and 24.0 μM), no toxicity was observed in 1.9 and 5.7 μM groups, whereas the delay of yolk sac absorption was found in 16.7% and 23.3% of zebrafish in 17.1 μM and 24.0 μM groups, respectively. No other toxicity was found in all of the FuBIG groups. By comparison, for zebrafish groups

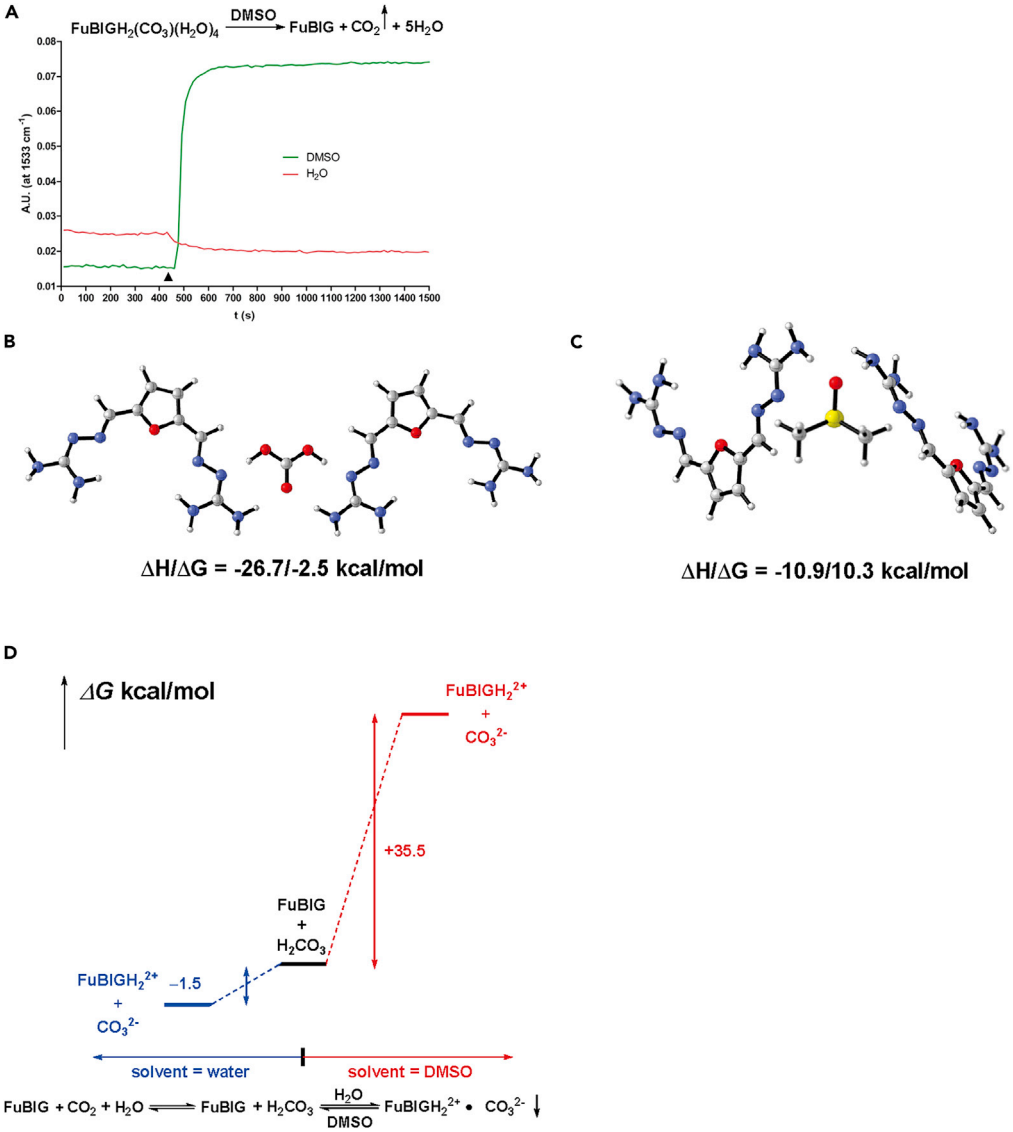

Figure 4. Spontaneous CO_2 release of FuBIG carbonate salt in DMSO

(A) Absorption intensity monitored at 1533 cm^{-1} (N—H) in liquid phase using React IR when FuBIG carbonate salt being added into DMSO and H_2O respectively. Triangle: representing the time point for the adding of FuBIG carbonate salt into the solvent.

(B) Binding energy of 2eq FuBIG with H_2CO_3.

(C) Binding energy of 2eq FuBIG with DMSO.

(D) Potential energy surface of the forming of $FuBIGH_2^{2+}$ and CO_3^{2-}.

treated with PyBIG (1.9, 5.7, 17.1, and 24.0 μM), no toxicity was observed in 1.9 μM group, whereas the delay of yolk sac absorption was found in 13.3% of zebrafish in 5.7 μM group. Moreover, it was observed that in 17.1 μM group treated with PyBIG, 6.7–30.0% of zebrafish developed renal edema, pericardium edema, delay of yolk sac absorption, lack and slowing down of blood flow, respectively. Further increment of PyBIG concentration to 24.0 μM, more serious toxic responses was observed with 10.0% of deaths occurred. In addition, FuBIG was found to be less toxic than PyBIG in embryo toxicity assay (for FuBIG: MNLC = 26.7 μM, LC_{10} = 55.9 μM; for PyBIG: MNLC = 15.8 μM, LC_{10} = 26.7 μM. Figures 5C and 5D). Notably, target organ toxicity tests of FuBIG and PyBIG in the same concentrations (1.8, 5.3, 15.8, and 26.7 μM) also revealed that the FuBIG has less embryo toxicity than PyBIG. The above-mentioned results suggested that the biomass-derived CO_2 sorbent might be more eco-friendly and more favorable in biocompatibility.

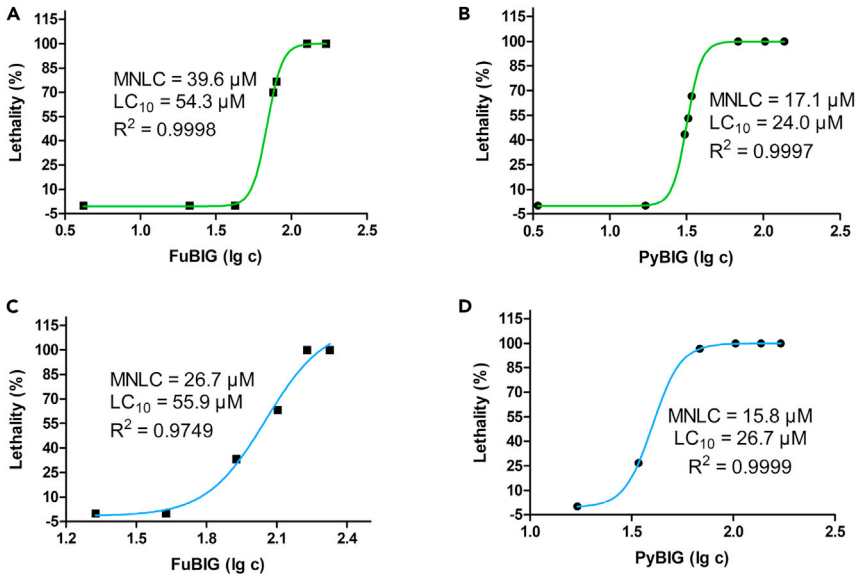

Figure 5. Biocompatibility assay of FuBIG and PyBIG in zebrafish

(A) Acute toxicity test of FuBIG with lethality (%) versus log function of concentration (μM) plots.

(B) Acute toxicity test of PyBIG with lethality (%) versus log function of concentration (μM) plots.

(C) Embryo toxicity test of FuBIG with lethality (%) versus log function of concentration (μM) plots.

(D) Embryo toxicity test of PyBIG with lethality (%) versus log function of concentration (μM) plots.

Conclusion

In summary, based on the concept of BBDAC, the biomass-based facile synthesis and comprehensive evaluation of the CO_2 chemical sorbent FuBIG are reported. Two binding modes with nine hydrogen bonds between FuBIG, CO_2 (as CO_3^{2-}), and H_2O were determined by single-crystal X-ray diffraction analysis. The stepwise and overall thermodynamic and kinetic parameters for CO_2 absorption and heat release have been obtained through van't Hoff analysis, TGA, DSC and *in situ* reaction analysis. The reaction for CO_2 absorption has an overall enthalpy value (ΔH_7) of −116.10 kJ/mol, and an overall equilibrium constant (K_7) of 5.97×10^4, showing that the absorption of CO_2 in aqueous solution of FuBIG is highly advantageous. Moreover, the reaction for CO_2 heat release of $FuBIGH_2(CO_3)(H_2O)_4$ displayed a relatively lower energy requirement with an enthalpy value (ΔH_8) of 209.31 kJ/mol. Besides, a simple and intuitive symbol for the evaluation of CO_2 sorbents, namely, the [R_s] value which was defined as the solubility ratio between sorbents and their carbonate salts was proposed in this study ([R_s] = 43.12 for FuBIG, 7.97 for PyBIG, and 1.60 for GBIG, respectively, at 25°C). In addition, React IR analysis showed that the CO_2 absorption process was consistent with the second-order reaction kinetics with a rate constant (k) of 4.8102×10^{-4} L/mol·s at 25°C, whereas the isothermal TGA analysis demonstrated that the kinetic characters for the release of CO_2 and H_2O from FuBIG carbonate salt was in line with the geometrical phase-boundary model. Notably, it was found that the spontaneous CO_2 release of FuBIG carbonate salt occurred in DMSO, which might represent a near-zero-energy technique for DAC, this amazing process for spontaneous CO_2 release in DMSO was further elucidated by DFT calculations. Finally, the acute toxicity and embryo toxicity assay in zebrafish model displayed that the biomass-derived CO_2 sorbent of FuBIG was more favorable in terms of biocompatibility. Further investigations to develop more efficient biomass-derived sorbents and researches on structure-property relationships are underway in our group.

Limitations of the study

This study designed and synthesized an iminoguanidine type CO_2 sorbent, the FuBIG, starting from the biomass-derived platform compound DFF as the core structure. However, the side chain of iminoguanidine (transformed from aminoguanidine) was not biomass-sourced at present. Technically speaking, the aminoguanidine could be biomass-sourced when it is needed (see Figure S1 for details). In addition, the capacity of FuBIG decreases by 7% within 10 cycles, showing an insufficient efficiency in CO_2 capture/release and sorbent regeneration process. Considering that the weight loss in sample transfer procedure was

inevitable, especially at a laboratory scale, it is possible that when the experiment is performed at a large-scale, the weight loss in sample transfer process would be greatly reduced. Furthermore, techno-economic analysis and life cycle analysis are warranted for future work.

Resource availability

Lead contact

Further information and requests for resources should be directed to and will be fulfilled by the lead contact, Yong Zou (zouyong3@mail.sysu.edu.cn).

Materials availability

Full experimental procedures are provided in the Supplemental Information.

Data and code availability

The accession numbers for FuBIGH$_2$(CO$_3$) (H$_2$O)$_4$ is CCDC: 2038310.

METHODS

All methods can be found in the accompanying transparent methods supplemental file.

SUPPLEMENTAL INFORMATION

Supplemental information can be found online at https://doi.org/10.1016/j.isci.2021.102263.

ACKNOWLEDGMENTS

This project was supported by the National Key Research and Development Project of China (2016YFA0602900), the National Natural Science Foundation of China (21272280), Guangdong Provincial Key Laboratory of Construction Foundation (2019B030301005), STPGC (201604020125), and ISRTIPZC (2015-224). We are thankful to Prof. Albert S. C. Chan at SYSU for guidance and help.

AUTHOR CONTRIBUTIONS

Y.Z. designed and supervised the whole project. Q.Z. synthesized and characterized the compound, designed and completed the experiments, and analyzed the data. Q.Z. and Y.Z. wrote the manuscript. X.S. and Y.J. synthesized the compounds (including the *O*-aryl carbamate) and helped in maintaining the devices. Y.L. and Z.K. performed the DFT study. All the authors were actively involved in the discussion, analysis, and revision.

DECLARATION OF INTERESTS

The authors declare no competing interests.

Received: November 27, 2020
Revised: February 5, 2021
Accepted: February 26, 2021
Published: April 23, 2021

REFERENCES

Anderson, S.E., Bart, R.R., Kennedy, M.C., MacDonald, A.J., Moritz, M.A., Plantinga, A.J., Tague, C.L., and Wibbenmeyer, M. (2018). The dangers of disaster-driven responses to climate change. Nat. Clim. Change *8*, 651–653.

Arias, P.L., Cecilia, J.A., Gandarias, I., Iglesias, J., Granados, M.L., Mariscal, R., Morales, G., Moreno-Tost, R., and Maireles-Torres, P. (2020). Oxidation of lignocellulosic platform molecules to value-added chemicals using heterogeneous catalytic technologies. Catal. Sci. Technol. *10*, 2721–2757.

Bajamundia, C.J.E., Koponenb, J., Ruuskanenb, V., Elfvinga, J., Kosonenb, A., Kauppinena, J., and Aholab, J. (2019). Capturing CO_2 from air: Technical performance and process control improvement. J. CO_2 Util. *30*, 232–239.

Boyd, P.G., Chidambaram, A., García-Díez, E., Ireland, C.P., Daff, T.D., Bounds, R., Gładysiak, A., Schouwink, P., Moosavi, S.M., Maroto-Valer, M.M., et al. (2019). Data-driven design of metal–organic frameworks for wet flue gas CO_2 capture. Nature *576*, 253–256.

Brethomé, F.M., Williams, N.J., Seipp, C.A., Kidder, M.K., and Custelcean, R. (2018). Direct air capture of CO_2 via aqueous-phase absorption and crystalline-phase release using concentrated solar power. Nat. Energy *3*, 553–559.

Bui, M., Adjiman, C.S., Bardow, A., Anthony, E.J., Boston, A., Brown, S., Fennell, P.S., Fuss, S., Galindo, A., Hackett, L.A., et al. (2018). Carbon capture and storage (CCS): the way forward. Energy Environ. Sci. *11*, 1062–1176.

Burant, A., Lowry, G.V., and Karamalidis, A.K. (2017). Measurement and modeling of setschenow constants for selected hydrophilic compounds in NaCl and $CaCl_2$ simulated carbon storage brines. Acc. Chem. Res. *50*, 1332–1341.

Carroll, J.J., Slupsky, J.D., and Mather, A.E. (1991). The solubility of carbon dioxide in water at low pressure. J. Phys. Chem. Ref. Data *20*, 1201.

Chheda, J.N., Huber, G.W., and Dumesic, J.A. (2007). Liquid-phase catalytic processing of biomass-derived oxygenated hydrocarbons to fuels and chemicals. Angew. Chem. Int. Ed. *46*, 7164–7183.

Cox, E., Spence, E., and Pidgeon, N. (2020). Public perceptions of carbon dioxide removal in the United States and the United Kingdom. Nat. Clim. Change *10*, 744–749.

Custelcean, R., Williams, N.J., Wang, X., Garrabrant, K.A., Martin, H.J., Kidder, M.K., Ivanov, A.S., and Bryantsev, V.S. (2020). Dialing in direct air capture of CO_2 by crystal engineering of bisiminoguanidines. ChemSusChem *13*, 6381–6390.

Davis, S.J., Lewis, N.S., Shaner, M., Aggarwal, S., Arent, D., Azevedo, I.L., Benson, S.M., Bradley, T., Brouwer, J., Chiang, Y., et al. (2018). Net-zero emissions energy systems. Science *360*, eaas9793.

Flores-Granobles, M., and Saeys, M. (2020). Minimizing CO_2 emissions with renewable energy: a comparative study of emerging technologies in the steel industry. Energy Environ. Sci. *13*, 1923–1932.

Gao, W., Liang, S., Wang, R., Jiang, Q., Zhang, Y., Zheng, Q., Xie, B., Toe, C.Y., Zhu, X., Park, S., et al. (2020). Industrial carbon dioxide capture and utilization: state of the art and future challenges. Chem. Soc. Rev.

Garrabrant, K.A., Williams, N.J., Holguin, E., Brethome, F.M., Tsouris, C., and Custelcean, R. (2019). Energy-efficient CO_2 capture from flue gas by absorption with amino acids and crystallization with a bis-iminoguanidine. Ind. Eng. Chem. Res. *58*, 10510–10515.

Ghatta, A.A., Wilton-Ely, J.D.E.T., and Hallett, J.P. (2019). Strategies for the separation of the furanic compounds HMF, DFF, FFCA, and FDCA from ionic liquids. ACS Sustain. Chem. Eng *7*, 16483–16492.

Gonzalez-Diaz, A., Jiang, L., Roskilly, A.P., and Smallbone, A.J. (2020). The potential of decarbonising rice and wheat by incorporating carbon capture, utilisation and storage into fertiliser production. Green. Chem. *22*, 882–894.

González-Zamora, E., and Ibarra, I.A. (2017). CO_2 capture under humid conditions in metal–organic frameworks. Mater. Chem. Front. *1*, 1471–1484.

He, Q., Shi, M., Liang, F., Xu, L., Ji, L., and Yan, S. (2019). Renewable absorbents for CO_2 capture: from biomass to nature. Greenhouse Gas Sci. Technol. *9*, 637–651.

Hohenberg, P., and Kohn, W. (1964). Inhomogeneous electron gas. Phys. Rev. *136*, B864–B871.

Holewinski, A., Sakwa-Novak, M.A., Carrillo, J.Y., Potter, M.E., Ellebracht, N., Rother, G., Sumpter, B.G., and Jones, C.W. (2017). Aminopolymer mobility and support interactions in Silica-PEI composites for CO_2 capture applications: a quasielastic neutron scattering study. J. Phys. Chem. B *121*, 6721–6731.

Huang, Xi., Liu, J., Sheng, J., Song, X., Du, Z., Li, M., Zhang, X., and Zou, Y. (2018). Decarboxylation of α,β-unsaturated aromatic lactones: synthesis of *E-ortho*-hydroxystilbenes from 3-arylcoumarins or isoaurone. Green. Chem. *20*, 804–808.

Jacobson, M.Z. (2019). The health and climate impacts of carbon capture and direct air capture. Energy Environ. Sci. *12*, 3567–3574.

Jin, S., Wu, M., Gordon, R.G., Aziz, M.J., and Kwabi, D.G. (2020). pH swing cycle for CO_2 capture electrochemically driven through proton-coupled electron transfer. Energy Environ. Sci. *13*, 3706–3722.

Ji, T., Liu, C., Lu, X., and Zhu, J. (2018). Coupled chemical and thermal drivers in microwaves toward ultrafast HMF oxidation to FDCA. ACS Sustain. Chem. Eng *6*, 11493–11501.

Keith, D.W. (2009). Why capture CO_2 from the atmosphere? Science *325*, 1654–1655.

Kohn, W., and Sham, L.J. (1965). Self-consistent equations including exchange and correlation effects. Phys. Rev. *140*, A1133–A1138.

Lackner, K.S. (2003). A guide to CO_2 sequestration. Science *300*, 1677–1678.

Leclaire, J., and Heldebrant, D.J. (2018). A call to (green) arms: a rallying cry for green chemistry and engineering for CO_2 capture, utilisation and storage. Green. Chem. *20*, 5058–5081.

Li, G., Liu, Q., Xia, B., Huang, J., Li, S., Guan, Y., Zhou, H., Liao, B., Zhou, Z., and Liu, B. (2017). Synthesis of stable metal-containing porous organic polymers for gas storage. Eur. Polym. J. *91*, 242–247.

Luo, X., Song, X., Xiong, W., Li, J., Li, M., Zhu, Z., Wei, S., Chan, A.S.C., and Zou, Y. (2019). Copper-catalyzed C–H carbamoyloxylation of aryl carboxamides with CO_2 and amines at ambient condition. Org. Lett. *21*, 2013–2018.

Luterbacher, J.S., Alonsoa, D.M., and Dumesic, J.A. (2014). Targeted chemical upgrading of lignocellulosic biomass to platform molecules. Green. Chem. *16*, 4816–4838.

Ma, J., Du, Z., Xu, J., Chu, Q., and Pang, Y. (2011). Efficient aerobic oxidation of 5-hydroxymethylfurfural to 2,5-diformylfuran, and synthesis of a fluorescent material. ChemSusChem *4*, 51–54.

McCann, N., Maeder, M., and Hasse, H. (2011). A calorimetric study of carbamate formation. J. Chem. Thermodyn. *43*, 664–669.

National Research Council (2015). Climate Intervention: Carbon Dioxide Removal and Reliable Sequestration (The National Academies Press).

Pang, S.H., Lee, L., Sakwa-Novak, M.A., Lively, R.P., and Jones, C.W. (2017). Design of Aminopolymer Structure to enhance performance and stability of CO_2 sorbents: poly(propylenimine) vs poly(ethylenimine). J. Am. Chem. Soc. *139*, 3627–3630.

Pramanik, A., Khansari, M.E., Powell, D.R., Fronczek, F.R., and Hossain, M.A. (2014). Absorption of atmospheric CO_2 as carbonate inside the molecular cavity of a new tripodal hexaurea receptor. Org. Lett. *16*, 366–369.

Reiner, D.M. (2016). Learning through a portfolio of carbon capture and storage demonstration projects. Nat. Energy *1*, 15011.

Saha, B., and Omar, M.M.A. (2014). Advances in 5-hydroxymethylfurfural production from biomass in biphasic solvents. Green. Chem. *16*, 24–38.

Sanz-Pérez, E.S., Murdock, C.R., Didas, S.A., and Jones, C.W. (2016). Direct capture of CO2 from ambient air. Chem. Rev. *116*, 11840–11876.

Sarazen, M.L., and Jones, C.W. (2017). Insights into Azetidine Polymerization for the preparation of poly(propylenimine)-based CO_2 adsorbents. Macromolecules *50*, 9135–9143.

Seipp, C.A., Williams, N.J., Kidder, M.K., and Custelcean, R. (2017). CO_2 capture from ambient air by crystallization with a guanidine sorbent. Angew. Chem. Int. Ed. *56*, 1042–1045.

Serrano-Ruiz, J.C., Luque, R., and Sepúlveda-Escribano, A. (2011). Transformations of biomass-derived platform molecules: from high added-value chemicals to fuels*via* aqueous-phase processing. Chem. Soc. Rev. *40*, 5266–5281.

Sha, F., Zhu, N., Bai, Y., Li, Q., Guo, B., Zhao, T., Zhang, F., and Zhang, J. (2016). Controllable synthesis of various $CaCO_3$ morphologies based on a CCUS idea. ACS Sustain. Chem. Eng *4*, 3032–3044.

Sheng, J., Xu, T., Zhang, E., Zhang, X., Wei, W., and Zou, Y. (2016). Synthesis of coumestrol and aureol. J. Nat. Prod. *79*, 2749–2753.

Shi, X., Xiao, H., Azarabadi, H., Song, J., Wu, X., Chen, X., and Lackner, K.S. (2020). Sorbents for the direct capture of CO_2 from ambient air. Angew. Chem. Int. Ed. *59*, 6984–7006.

Solanki, B.S., and Rode, C.V. (2019). Selective hydrogenation of 5-HMF to 2,5-DMF over a magnetically recoverable non-noble metal catalyst. Green. Chem. *21*, 6390–6406.

Strube, R., Pellegrini, G., and Manfrida, G. (2011). The environmental impact of post-combustion CO_2 capture with MEA, with aqueous ammonia, and with an aqueous ammonia-ethanol mixture for a coal-fired power plant. Energy *36*, 3763–3770.

Sutherland, B.R. (2019). Pricing CO2 direct air capture. Joule *3*, 1571–1573.

Thakkar, H., Issa, A., Rownaghi, A.A., and Rezaei, F. (2017). CO_2 Capture from air using amine-functionalized kaolin-based zeolites. Chem. Eng. Technol. *40*, 1999–2007.

Trickett, C.A., Helal, A., Al-Maythalony, B.A., Yamani, Z.H., Cordova, K.E., and Yaghi, O.M. (2017). The chemistry of metal–organic frameworks for CO_2 capture, regeneration and conversion. Nat. Rev. Mater. *2*, 17045.

Wang, W., Zhou, M., and Yuan, D. (2017). Carbon dioxide capture in amorphous porous organic polymers. J. Mater. Chem. A *5*, 1334–1347.

Wang, X. (2016). CO2 Capture and Utilization (Chemical Industry Press).

Wang, X., Conway, W., Burns, R., McCann, N., and Maeder, M. (2010). Comprehensive study of the hydration and dehydration reactions of carbon dioxide in aqueous solution. J. Phys. Chem. A *114*, 1734–1740.

Williams, N.J., Seipp, C.A., Brethomé, F.M., Ma, Y., Ivanov, A.S., Bryantsev, V.S., Kidder, M.K., Martin, H.J., Holguin, E., and Custelcean, R. (2019). CO_2 capture via crystalline hydrogen-bonded bicarbonate dimers. Chem *5*, 719–730.

Wu, W., Zou, Y., Chen, Y., Li, J., Lv, Z., Wei, W., Huang, T., and Liu, X. (2012). Bio-based synthesis of secondary arylamines from (−)-shikimic acid. Green. Chem. *14*, 363–370.

Yang, Z., Chen, H., Li, B., Guo, W., Jie, K., Sun, Y., Jiang, D., Popovs, I., and Dai, S. (2019). Topotactic synthesis of phosphabenzene-functionalized porous organic polymers: efficient ligands in CO_2 conversion. Angew. Chem. Int. Ed. *58*, 13763–13767.

Zhai, H., Ou, Y., and Rubin, E.S. (2015). Opportunities for decarbonizing existing U.S. coal-fired power plants via CO_2 capture, utilization and storage. Environ. Sci. Technol. *49*, 7571–7579.

Zhang, E., Xu, T., Wang, D., Huang, T., Yuan, M., Li, J., and Zou, Y. (2014a). Consecutive reactions between methyl 3-dehydroshikimiate, amines and 1,2-dichloroalkanes under microwave conditions: a practical, one-pot construction of N-substituted dihydrobenzoxazines. RSC Adv. *4*, 10022–10027.

Zhang, E., Xu, T., Wei, W., Huang, T., Yuan, M., Zeng, W., and Zou, Y. (2014b). Cascade reaction between methyl 3-dehydroshikimate, arylamines, and 2-chloroalkyl esters under microwave conditions: a practical and biomass-based synthesis of *N*-Aryl-1,4-benzoxazin-3-ones. Synthesis *46*, 1167–1176.

Zhang, E., Zhang, X., Cai, Y., Wang, D., Xu, T., Li, J., Yan, M., and Zou, Y. (2014c). Biomass-involved, facile and one-pot synthesis of *N*-aryl-2(3*H*)-benzoxazolones from methyl 3-dehydroshikimiate. RSC Adv. *4*, 39020–39029.

Zhang, E., Zhang, X., Wei, W., Wang, D., Cai, Y., Xu, T., Yan, M., and Zou, Y. (2015). A biomass-involved strategy for the synthesis of *N*-arylated dibenzo[*b*,*e*][1,4]oxazepin-11(5*H*)-ones, acridones, 7,12-dihydrodibenzo[*b*,*e*][1,4]oxazocin-6*H*-ones and dibenzo[*b*,*f*]azepin-10(11*H*)-ones. RSC Adv. *5*, 5288–5294.

Zhang, Z., and Huber, G.W. (2018). Catalytic oxidation of carbohydrates into organic acids and furan chemicals. Chem. Soc. Rev. *47*, 1351–1390.

Zhao, H., Holladay, J.E., Brown, H., and Zhang, Z.C. (2007). Metal chlorides in ionic liquid solvents convert sugars to 5-hydroxymethylfurfural. Science *316*, 1597–1600.

Zhao, J., Chen, X., Du, Y., Yang, Y., and Lee, J.M. (2018). Vanadium-embedded mesoporous carbon microspheres as effective catalysts for selective aerobic oxidation of 5-hydroxymethyl-2-furfural into 2, 5-diformylfuran. Appl. Catal. A *568*, 16–22.

Zhu, S., Guo, J., Wang, X., Wang, J., and Fan, W. (2017). Alcoholysis: a promising technology for conversion of lignocellulose and platform chemicals. ChemSusChem *10*, 2547–2559.

Zou, L., Sun, Y., Che, S., Yang, X., Wang, X., Bosch, M., Wang, Q., Li, H., Smith, M., Yuan, S., et al. (2017). Porous organic polymers for post-combustion carbon capture. Adv. Mater. *29*, 1700229.

iScience, Volume *24*

Supplemental information

Design, synthesis, and physicochemical study of a biomass-derived CO_2 sorbent 2,5-furan-bis(iminoguanidine)

Qianzhong Zhang, Yi Jiang, Yinwu Li, Xianheng Song, Xiang Luo, Zhuofeng Ke, and Yong Zou

Supplemental Information

Transparent Methods

Experimental

Common reagents used in the synthesis were obtained commercially and used without further purification unless otherwise specified. All water used was deionized (18 mΩ). The ^{1}H NMR and ^{13}C NMR spectra were recorded using TMS as the internal standard on a Bruker BioSpin GmbH spectrometer at 400, 500 MHz respectively. UV-vis spectra were measured in 10-mm-path-length quartz cuvettes using a UV-2600 (SHIMADZU). pH measurements were conducted with a PHS-3E pH meter (Shanghai INESA Scientific Instrument CO., ltd) using an E-301F pH electrode. PXRD measurements were performed with X-ray single crystal diffractometer (Xcalibur Nova). 12423 diffraction points and 5860 independent diffraction points (R_{int} = 0.0204, R_{sigma} = 0.0213) were collected within the range of $2\theta_{max}$ = 134° at T = 100 K using Cu-Kα ray (λ = 1.54184 Å) was used as a light source. The crystal structure was analyzed by XS (Sheldrick, 2008) and refined by SHELXL (Sheldrick, 2015). TGA was under a nitrogen atmosphere using a STA 409PC (NETZSCH). DSC measurements were conducted under nitrogen with a DSC 3 (METTLER TOLEDO). In situ reaction analysis was conducted with a React IR 15 (METTLER TOLEDO). Acute toxicity and embryo toxicity experiment in zebrafish were observed with stereomicroscope (SZX7, OLYMPUS, Japan), and photos taken by CCD camera (VertA1, Shanghai Tusen Vivion Technology Co., Ltd, China). Sorbents were weighed with a precision electronic balance (CP214, OHAUS, USA).

Methods

Synthesis of FuBIG

2,5-furandialdehyde (12.4 g, 0.1 mol), aminoguanidine hydrochloride (22 g, 0.2 mol) and ethanol (100 mL) were added to a 250 mL round bottom flask fitted with a condenser. The mixture was heated at 70 °C with stirring for 8 h. After the reaction was ended, the reaction mixture was subjected to standing for 4h at 4 °C. The $FuBIGH_2Cl_2$ product was collected by vacuum filtration as a light yellow solid, washed with ethanol for three times, then was dried under vacuum. The procedure yielded 34.7 g (98% yield). The chloride salt recrystallized from ethanol to be used in pK_a experiment.

The above 2,5-furyldiiminoguanidine hydrochloride hydrate was put in a 250 mL round bottom flask, added with 50 ml of 2M sodium hydroxide aqueous solution, stirred for 0.5h at room temperature, then subjected to standing for 12h at 4 °C. Resulting yellow solid was collected by vacuum filtration and dried to obtain 22.66 g (96% yield) of FuBIG.

CO_2 capture from air using aqueous FuBIG

FuBIG (2.36 g, 10 mmol) was dissolved into 100mL of water and stirred for 12h at room temperature under the condition of sufficiently contacting with air to separate out a yellow solid. The yellow solid was filtered at reduced pressure and dried to obtain yellow powder (3.52 g, 95%), which was $FuBIGH_2(CO_3)(H_2O)_4$.

Single crystal X-ray diffraction

X-ray quality single crystals of $FuBIGH_2(CO_3)(H_2O)_4$ were obtained by preparing an aqueous solution of FuBIG (20 mL, 5 mM) in a 50 mL round bottom flask under ambient air, and let it at room temperature few days. 12423 diffraction points and 5860 independent diffraction points (R_{int} = 0.0204, R_{sigma} = 0.0213) were collected within the range of $2\theta_{max}$ = 134° at T = 100 K using Cu-Kα ray (λ = 1.54184 Å) was used as a light source. The crystal structure was analyzed by XS (Sheldrick, 2008) and refined by SHELXL (Sheldrick, 2015).

pK_a determination by potentiometric titrations

The variable temperature titrations of pK_a of FuBIG were done at the desired temperature using a circulating water bath. The electrode was calibrated by potassium hydrogen phthalate buffer (pH 4.00), mixed phosphate buffer (pH 6.86) and sodium tetraborate buffer (pH 9.18) respectively. A 50 mL ultrapure water solution containing FuBIG (5 mM), HCl (6 mM) and NaCl

background electrolyte (0.2 mM) was titrated with a standard 0.1 M NaOH solution using a 200 µL pipette. The potential readings were recorded 5 minutes after each NaOH addition to allow the solution to equilibrate. The volume and pH value of each titration were recorded. **Table S7** lists the pK_a values obtained in the 15-35 °C range.

Solubility measurements

The solubilities of FuBIG and $FuBIGH_2(CO_3)(H_2O)_4$ under variable temperature were determined by measuring the UV-Vis absorption spectra of the corresponding saturated ultrapure water solutions and comparing with a calibration curve obtained using solutions of $FuBIGH_2Cl_2$ of known concentrations. The $FuBIGH_2Cl_2$ aqueous solutions having the concentrations of 1.346×10^{-5} M, 2.690×10^{-5} M, 3.365×10^{-5} M, 6.730×10^{-5} M and 1.350×10^{-4} M respectively. The absorbance of the $FuBIGH_2Cl_2$ samples was recorded under the maximum absorption wavelength (**Table S3**).

Saturated solutions were prepared by suspending an excess of the crystalline solids in 10 mL H_2O inside reaction tube, and stirred for 24h inside a circulating water bath at different temperatures in the range of 15 to 35 °C. All measurements were run in triplicate. The average solubility values of FuBIG and $FuBIGH_2(CO_3)(H_2O)_4$ are reported respectively in **Table S4** and **S6**.

Determination of K_{sp} of $FuBIGH_2(CO_3)(H_2O)_4$

$$FuBIGH_2(CO_3)(H_2O)_4 \rightleftharpoons FuBIGH_2^{2+} + CO_3^{2-} + 4H_2O \quad (1)$$

$$HCO_3^- \rightleftharpoons CO_3^{2-} + H^+ \quad (2)$$

$$FuBIGH_2^{2+} \rightleftharpoons FuBIGH^+ + H^+ \quad (3)$$

$$FuBIGH^+ \rightleftharpoons FuBIG + H^+ \quad (4)$$

As the calculation of K_{sp} at 25°C for an example:

K_{sp} is the reaction equilibrium constant of equation 1. The concentration of $FuBIGH_2^{2+}$ and CO_3^{2-} in equilibrium and the activity coefficient ($\gamma_\pm$) at 25°C need be measured and calculated. The concentration of carbonate anion was calculated by equation 2 and mass balance, it was determined to be 0.0001331 M considering the pK_a of HCO_3^- is 10.32 and the pH of the saturated carbonate solution is 8.48.

The concentration of the $FuBIGH_2^{2+}$ cation was determined by taking into account of the measured solubility of $FuBIGH_2(CO_3)(H_2O)_4$ (0.009344 M), the pK_a values of FuBIG in 25 °C (7.57 (equation 3) and 8.71 (equation 4)) and the pH of the saturated solution is 8.48. The concentration of the ligand is: FuBIG 0.003214 M, $FuBIGH^+$ 0.005458 M, $FuBIGH_2^{2+}$ 0.0006715 M.

Ionic strength can be calculated and the value is 0.001609. The activity coefficients ($\gamma_\pm$) were estimated at 0.828 using the Debye-Huckel limiting law (Peiper and Pitzer, 1982; Stefánsson et al., 2013; Huang, 2010). The Values of K_{sp} at other temperature were calculated as the same measurement.

The pK_a of HCO_3^- and value of A in Debye-Huckel limiting law at 15-35 °C were obtained from previous references (Peiper and Pitzer, 1982; Huang, 2010). **Table S5** lists the pH of saturated $FuBIGH_2(CO_3)(H_2O)_4$ solution in the range of 15-35 °C. **Table S6** lists the K_{sp} values obtained in the range of 15-35 °C.

$$I = \frac{1}{2} \times \sum^n cz^2 = \frac{1}{2}(0.0001331 \times 2^2 + 0.0006715 \times 2^2) = 0.001609 \quad (5)$$

$$\lg \gamma_\pm = -A|Z^+Z^-|\sqrt{I} = -0.5115 \times 4 \times \sqrt{0.001609} = -0.08207 \quad (6)$$

$$K_{sp} = (\gamma_\pm)^2 \times [FuBIGH_2^{2+}] \times [CO_3^{2-}] = (0.828)^2 \times 0.0006715 \times 0.0001331 = 6.128 \times 10^{-8} \quad (7)$$

TGA measurements
The TGA was under a nitrogen atmosphere. The sample was ramped at 10 °C/min to 600 °C. For the isothermal measurement, FuBIG carbonate salt was ramped 5 °C/min to 50, 60, 70, 80, 90 °C and 10 °C/min to 100, 110 °C, then held the temperature for 180 min.

DSC measurements
DSC was conducted under a nitrogen atmosphere. The sample was measured in a temperature range of 30-200 °C and temperature ramp of 10 °C/min.

CO_2 absorption and release of FuBIG monitored by ReactIR
The infrared spectrum of FuBIG and FuBIG$H_2(CO_3)(H_2O)_4$ was collected through ReactIR. The peak at 1533 cm^{-1} is the characteristic N-H absorption of FuBIG, while the peak at 1365 cm^{-1} representing the wavenumber of the carbonate salt. The calibration curve was determined by FuBIG aqueous solutions having the concentrations of 0.15890 M and diluted 5, 10, 25 and 50 times respectively. The absorbance of the above concentration FuBIG solutions was measured in ReactIR.
FuBIG (2.83 g, 12 mmol) was added to a 100 mL three-necked flask and dissloved into 40 mL water at 25°C. One neck of flask was inserted into an on-line Infrared Dicomp Probe and fixed with a Teflon adapter. One data is collected every 0.5 min. After the absorbance is stabilized, a CO_2 balloon was inserted into the other mouth of the flask, and continued to stir until FuBIG was completely converted into FuBIG$H_2(CO_3)(H_2O)_4$. Then the mixture was heated to 70 °C, FuBIG$H_2(CO_3)(H_2O)_4$ precipitate released CO_2 and converted to FuBIG aqueous solution again.

Accelerated aging test of FuBIG$H_2(CO_3)(H_2O)_4$
FuBIG$H_2(CO_3)(H_2O)_4$ (0.1850 g, 0.5 mmol) was put on a crystallization dish (24.1800 g). Then placed the crystallization dish into the oven and heated to 110 °C for one week. The weight change of FuBIG$H_2(CO_3)(H_2O)_4$ was measured every 6 hours.

CO_2 separation cycles
FuBIG (9.5 g, 0.04 mol) was dissolved into 100 mL ultrapure water in a 250 mL round bottom flask and marked liquid level. The absorbance of FuBIG at 368 nm was measured to be substituted into the standard equation to calculate the concentration. Then the CO_2 balloon was bubbled through the solution for 1 hour. A yellow precipitate started to form after 5 min. The yellow solid was collected by vacuum filtration. The filtrate was collected and analyzed by UV-Vis spectroscopy to determine the concentration of FuBIG left in solution. The filtrate was saved for the next cycle. The precipitate was placed in a crystallization dish and heated for 4 hours in an oven at 100 °C. The regenerated FuBIG was redissolved into the filtrate saved from the previous cycle and the ultrapure water was added to the mark. And the resulting FuBIG solution was recycled. Overall, ten consecutive cycles had been run.

CO_2 utilization
N-(quinolin-8-yl)benzamide (1.0 g, 4 mmol), diethylamine (827 μL, 8 mmol), DBU (1.79 mL, 12 mmol), cuprous iodide (0.15 g, 0.8 mmol) and manganese dioxide (0.70 g, 8 mmol) were added to a reaction tube, and dissolved with 20 mL DMF. FuBIG$H_2(CO_3)(H_2O)_4$ (2.22 g, 6 mmol) was added to another reaction tube (Luo et al., 2019). The above-mentioned devices were connected via a breather pipe. FuBIG$H_2(CO_3)(H_2O)_4$ was heated at 80 °C to release CO_2. The copper-catalyzed, one-pot three-component oxidative coupling of benzoylaminoquinoline with CO_2 and diethylamine occurred under standard conditions, affording the corresponding *O*-aryl carbamate (2-(quinolin-8-ylcarbamoyl)phenyl diethylcarbamate) in 73% yield (**Figure S24**).

DFT computational
All reported structures were optimized by the density functional theory (DFT) (Kohn and Sham, 1965; Hohenberg and Kohn, 1964) with the B3LYP functional (Vosko et al., 1980; Lee et al., 1988; Becke, 1993) with 6-31G (d, p) basis sets (Petersson et al., 1988, 1991) in the gas phase. Based on the recent studies by Grimme, the empirical dispersion correction was considered to be important in accurate prediction of the reaction free energy (Chakraborty et

al., 2014). Hence, the D3 version of Grimme's dispersion correction with the original D3 damping function was considered in structure optimizations and energy calculations (Grimme et al., 2010). Frequency analysis calculations of optimized structures were performed at the same level of theory to characterize the structures to be minima (no imaginary frequency). Based on the B3LYP-D/6-31G (d, p) optimized geometries, the energy results were further refined by calculating the single point energy at the B3LYP-D/6-311++G (d, p) (Petersson et al., 1988, 1991) level of theory. The bulky solvation effects were simulated by SMD (Marenich et al., 2009) continuum solvent mode at the B3LYP-D/6-311++G (d, p) level of theory, with water (ε = 78.4) and DMSO (ε = 46.8), respectively, according to their corresponding reaction conditions. All the calculations were performed with the Gaussian 09 program (Frisch et al., 2013). The 3D optimized structures were displayed by CYLview visualization program (Legault, 2009).

Zebrafish handling

Adult AB strain zebrafish were fed with live brine shrimp twice daily and dry flake once a day. The culture temperature was controlled by aquaculture facility with a standard 14 h/10 h light/dark photoperiod (Westerfield, 1995). Four to five pairs of zebrafish were set up for nature mating every time. On average, 200–300 embryos were generated. Embryos were maintained at 28 °C in fish water (0.2% Instant Ocean Salt in deionized water, pH 6.9-7.2, conductivity 480-510 μS/cm and hardness 53.7-71.6 mg/L $CaCO_3$). The embryos were washed and staged at 6 h post-fertilization (hpf) and 24 hpf (Kimmel et al., 1995). Zebrafish were housed in Hunter Biotechnology, Inc., which is accredited by the Association for Assessment and Accreditation of Laboratory Animal Care (AAA LAC) International.

Determination of maximum non-lethal concentration (MNLC) and LC_{10}

Zebrafish larvae were treated with FuBIG or PyBIG from 48 to 120 hpf for the acute toxicity, from 4 to 120 hpf for the embryonic toxicity assay (He et al., 2013; Zhu et al., 2014). Mined as those lacking an observable heartbeat under a dissecting stereomicroscope. Seven concentrations were used for each sample. If LC_{10} (10% lethal concentration) and MNLC were not reached, additional testing concentrations up to 2000 μM and down to 0.001 μM were tested. Mortality curves were generated using Origin 8.0 (OriginLab, USA). MNLC and LC_{10} were estimated from this curve.

Identification of target organs

Four concentrations (1/9 MNLC, 1/3 MNLC, MNLC and LC_{10}) were used to identify the toxicity target organs. Zebrafish larvae were treated with samples from 48 to 120 hpf. At the end of treatment, zebrafish from each group were randomly selected for visua observation and image acquisition. Major zebrafish organs and tissues were visually assessed, and toxic target organs were identified based on morphological abnormalities.

After treatment, the heart, brain, eyes, liver, intestine, spine, and behaviours of each fish were observed under the microscope. The occurrence of edema, hemorrhage, and thrombosis were also observed in the animals.

Embryo toxicity

Four concentrations (1/9 MNLC, 1/3 MNLC, MNLC and LC_{10}) were used to identify the embryonic toxicity. Zebrafish larvae were treated with samples from 4 to 120 hpf. At the end of treatment, zebrafish from each group were randomly selected for visual observation and image acquisition. Embryos were daily observed up to 120 h with the dissecting stereomicroscope (SZX7, OLYMPUS, Japan), recording the four apical observations as indicators of lethality: coagulation of fertilized eggs, lack of somite formation, lack of detachment of the tailbud from the yolk sac, and lack of heartbeat. During the exposure period, developmental alterations, teratological parameters, and percentage of hatching were also recorded. Major zebrafish organs and tissues were visually assessed, and toxic target organs were identified based on morphological abnormalities. After treatment, the heart, brain, eyes, liver, intestine, spine, and behaviors of each fish were observed under the microscope. The occurrence of edema, hemorrhage, and thrombosis were also observed in the animals.

Supplemental Figures

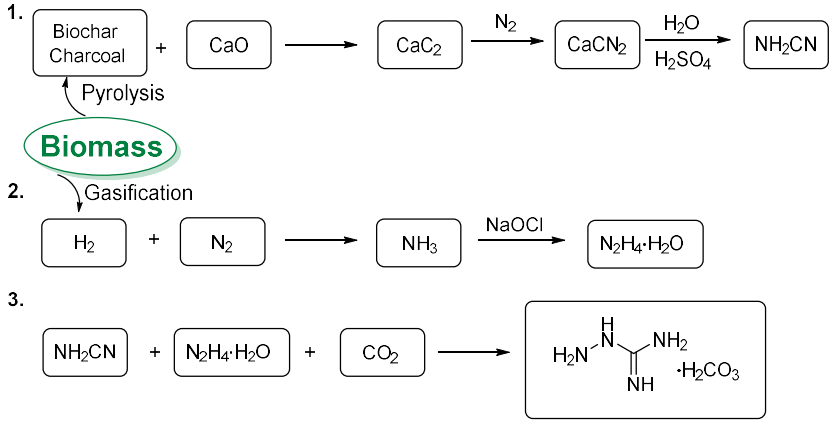

Figure S1. Synthetic routes of biomass derived aminoguanidine. Related to Figure 1.

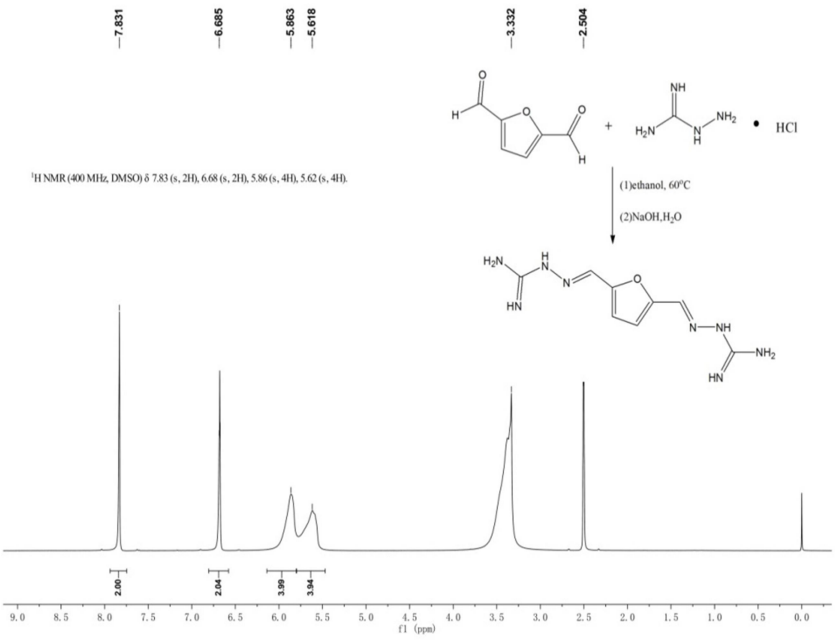

Figure S2. ^{1}H-NMR Spectrum of FuBIG in DMSO-d_6. Related to Figure 2.

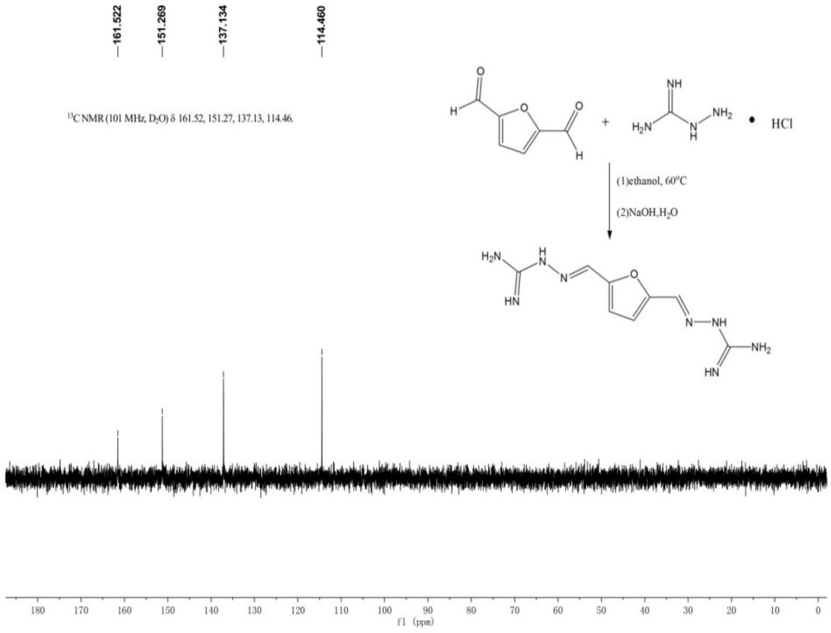

Figure S3. ^{13}C-NMR Spectrum of FuBIG in DMSO-d_6. Related to Figure 2.

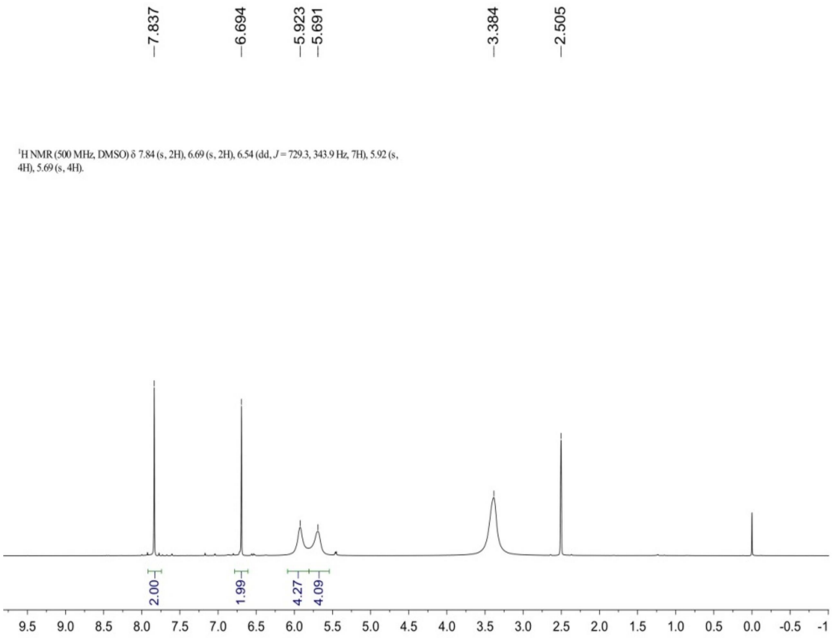

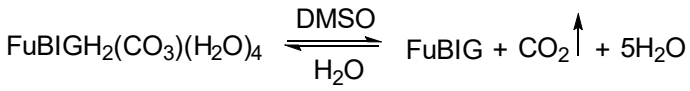

Figure S4. ^{1}H-NMR spectrum of FuBIG$H_2(CO_3)(H_2O)_4$ in DMSO-d_6 showing a pattern fully identical with that of FuBIG in DMSO-d_6. Related to Figure 4.

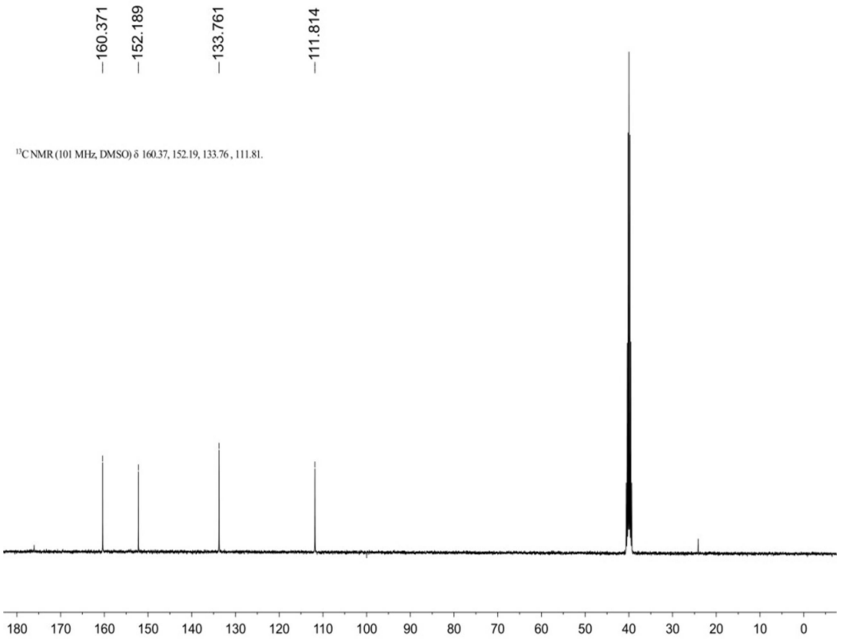

$$FuBIGH_2(CO_3)(H_2O)_4 \underset{H_2O}{\overset{DMSO}{\rightleftharpoons}} FuBIG + CO_2\uparrow + 5H_2O$$

Figure S5. ^{13}C-NMR spectrum of $FuBIGH_2(CO_3)(H_2O)_4$ in DMSO-d_6 showing a pattern fully identical with that of FuBIG in DMSO-d_6. Related to Figure 4.

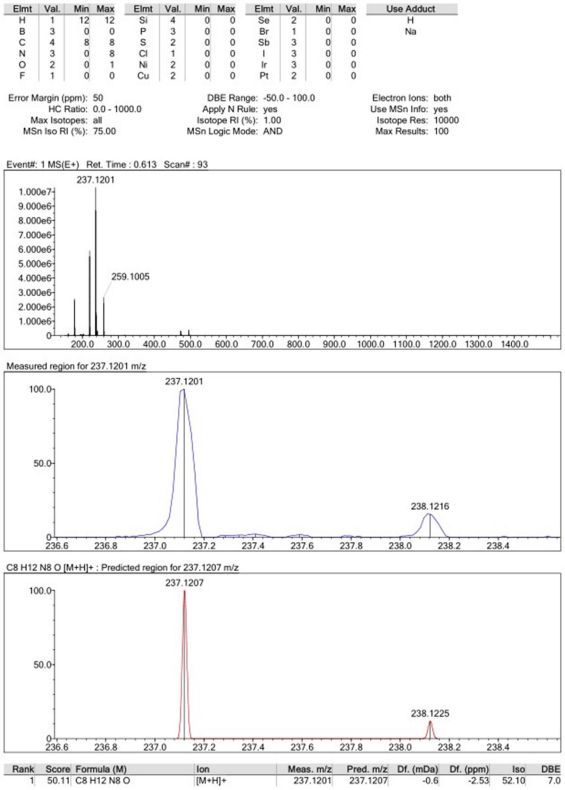

Figure S6. HRMS spectrum of FuBIG. Related to Figure 2.

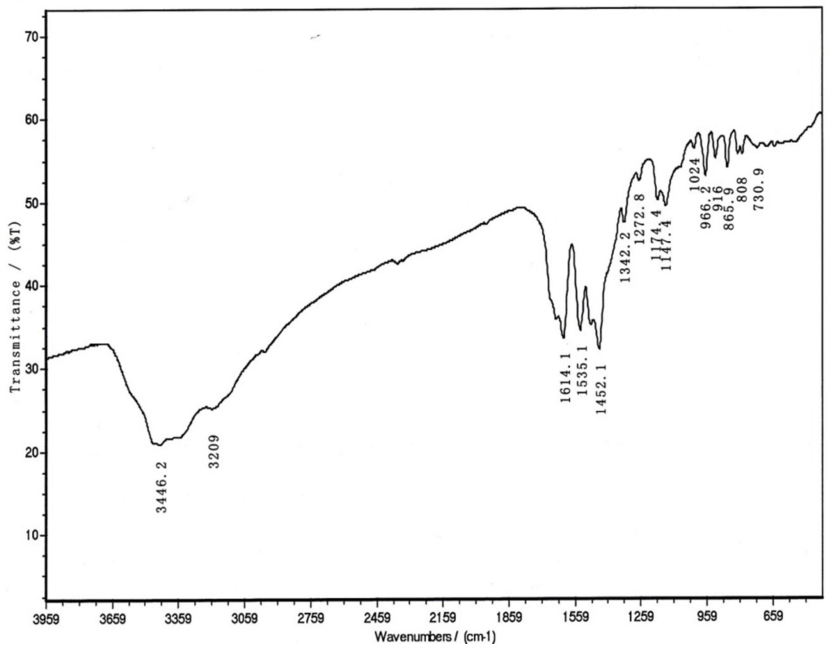

Figure S7. FTIR spectrum of FuBIG. Related to Figure 2.

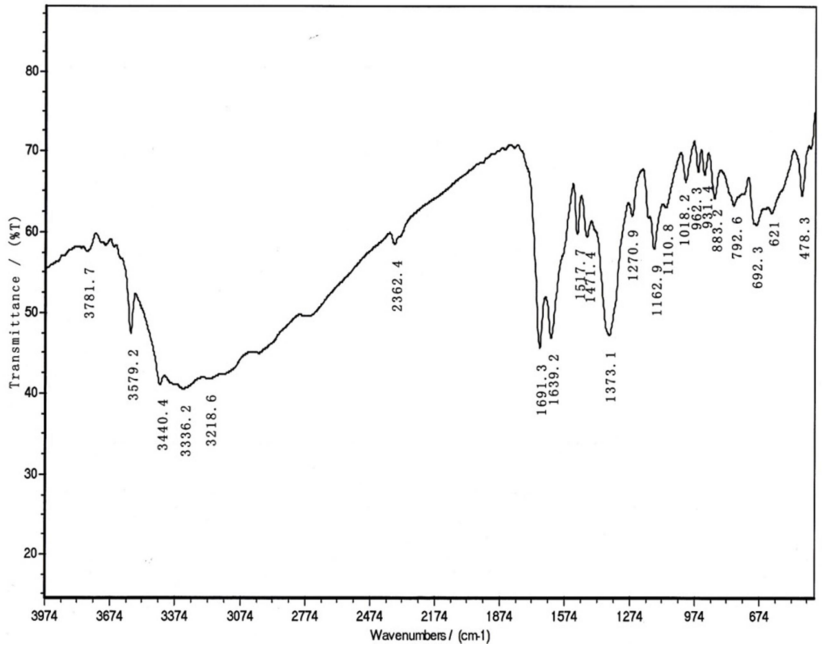

Figure S8. FTIR spectrum of $FuBIGH_2(CO_3)(H_2O)_4$. Related to Figure 2.

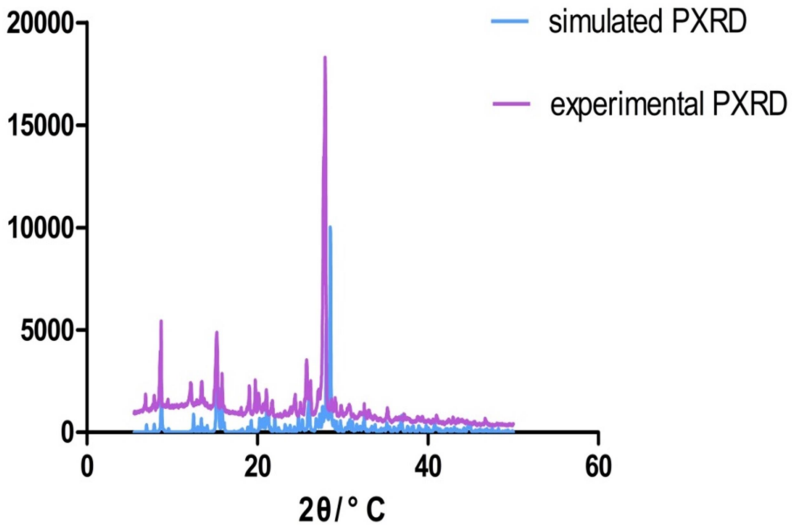

Figure S9. Overlay of the experimental PXRD pattern of the bulk crystalline product (purple) and the simulated PXRD pattern from the single-crystal X-ray data (blue). Related to Figure 2.

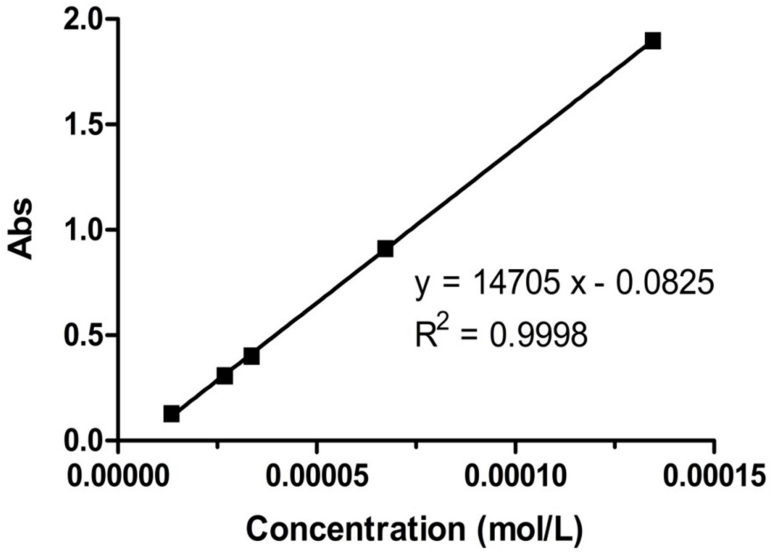

Figure S10. Standard absorption curve of $FuBIGH_2Cl_2$ at 368 nm. Related to Table 1.

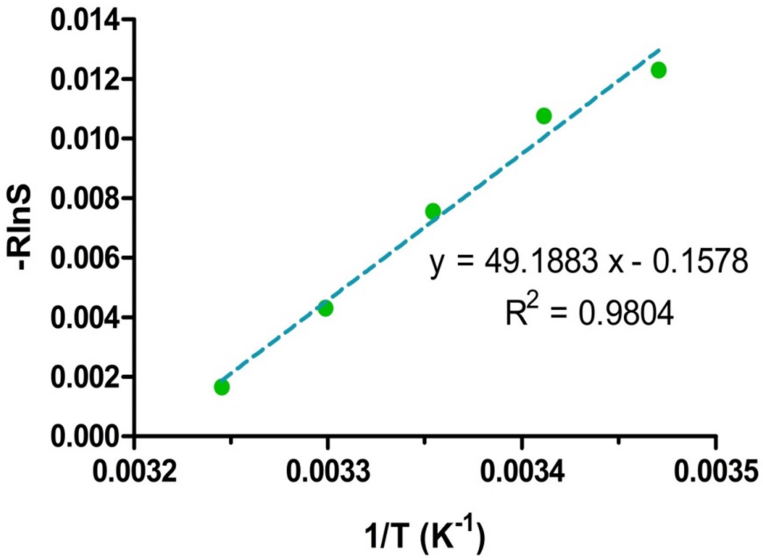

Figure S11. Van't Hoff analysis of FuBIG solubility. Related to Table 1. According to the equation : -Rln K = - ΔH/T + ΔS, the slope of the fitted equation is the value of ΔH in this reaction.

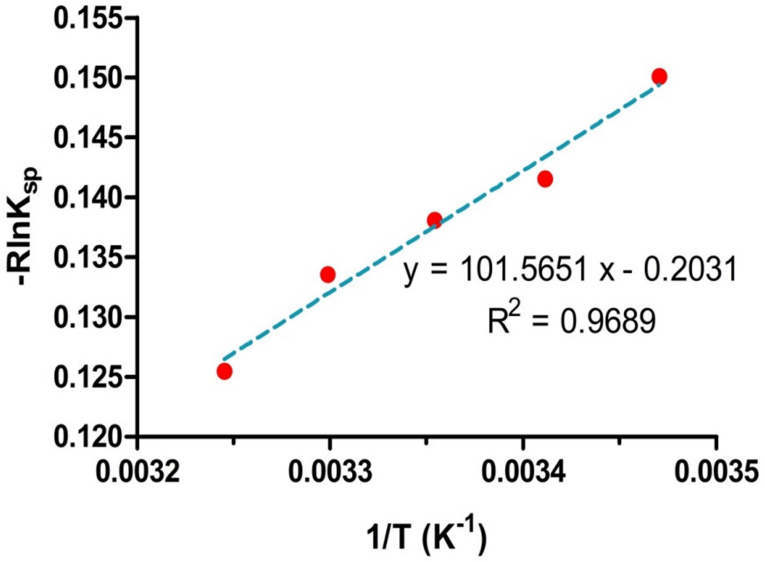

Figure S12. Van't Hoff analysis of solution equilibrium constant of $FuBIGH_2(CO_3)(H_2O)_4$. Related to Table 1. K_{sp} of $FuBIGH_2(CO_3)(H_2O)_4$ at different temperature was calculated respectively to ensure the accuracy of ΔH of $FuBIGH_2(CO_3)(H_2O)_4$ crystallization.

(a)

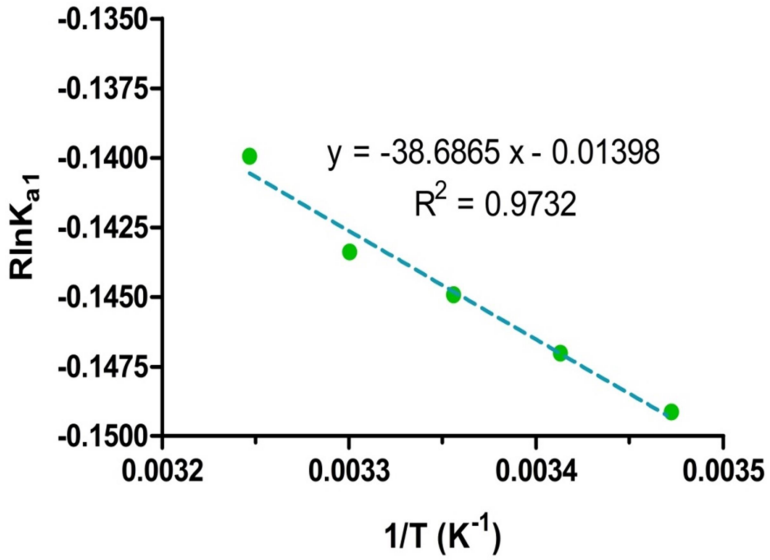

(b)

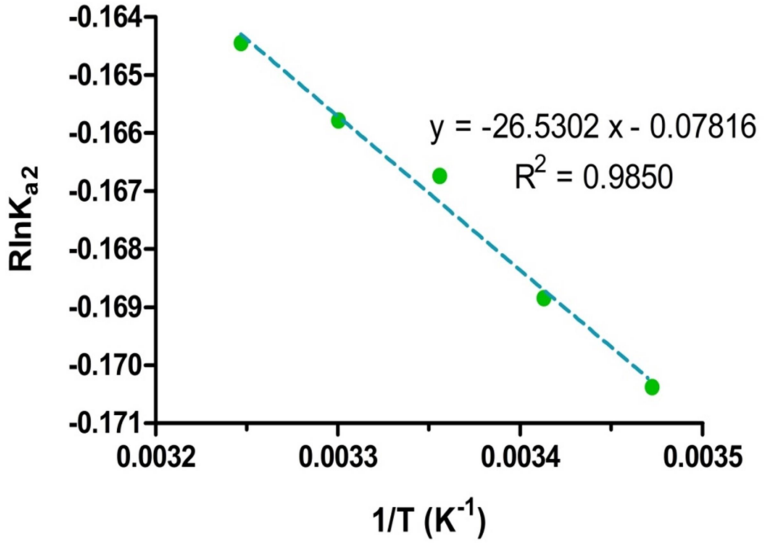

Figure S13. Van't Hoff analysis of FuBIGH$_2^{2+}$ deprotonation. Related to Table 1. (a) Van't Hoff analysis of pK$_{a1}$ of FuBIG. (b) Van't Hoff analysis of pK$_{a2}$ of FuBIG.

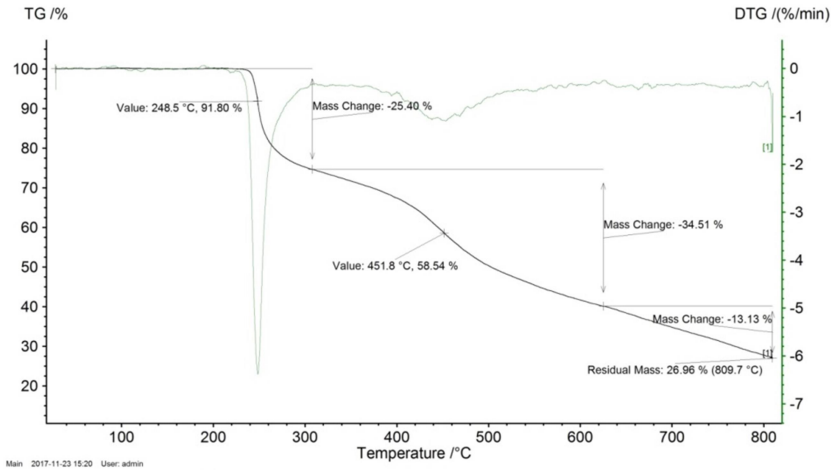

Figure S14. Temperature-ramped TGA plots showing the thermostability of FuBIG. Related to Figure 3.

(a)

(b)

Figure S15. Photos of $FuBIGH_2(CO_3)(H_2O)_4$ crystals under the microscope. Related to Figure 3. (a) $FuBIGH_2(CO_3)(H_2O)_4$ crystals before heating. (b) The crystals of $FuBIGH_2(CO_3)(H_2O)_4$ had been heated in an oven at 120°C for 1h, the crystals transformed to FuBIG and changed their appearance from transparent to opaque. The scale represents 25 μm.

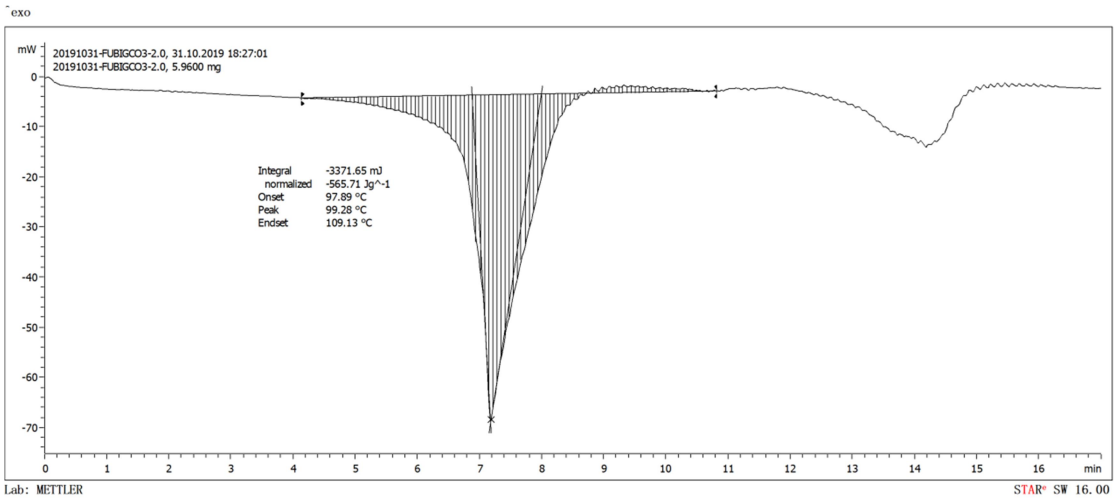

Figure S16. Differential scanning calorimetry (DSC) for CO_2 release of $FuBIGH_2(CO_3)(H_2O)_4$. Related to Table 1.

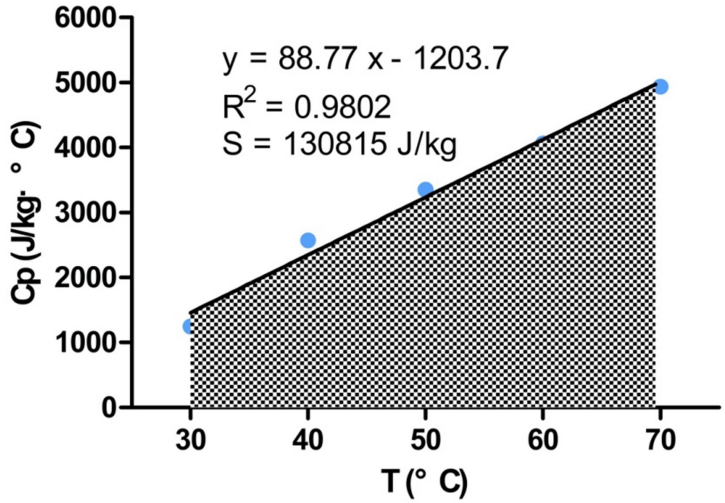

Figure S17. Specific heat capacity of $FuBIGH_2(CO_3)(H_2O)_4$ as a function of temperature, measured by DSC. Related to Table 1. The area bounded by the curve and the abscissa is the enthalpy of the specific heat capacity.

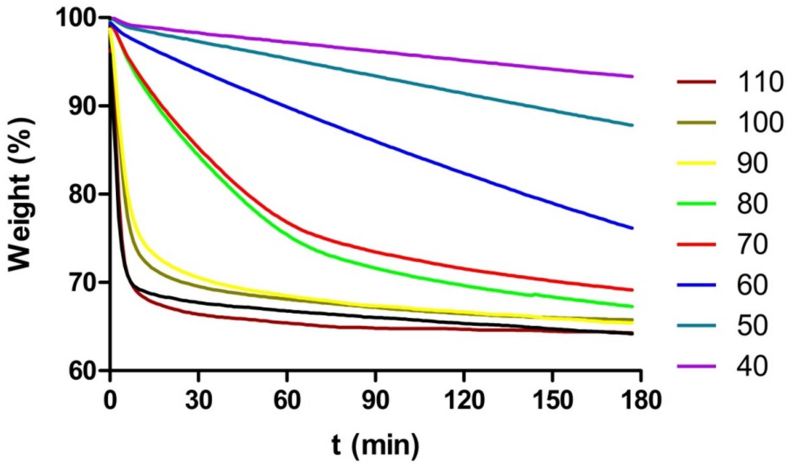

Figure S18. Isothermal TGA data of $FuBIGH_2(CO_3)(H_2O)_4$ at the range of 40-110°C. Related to Figure 3.

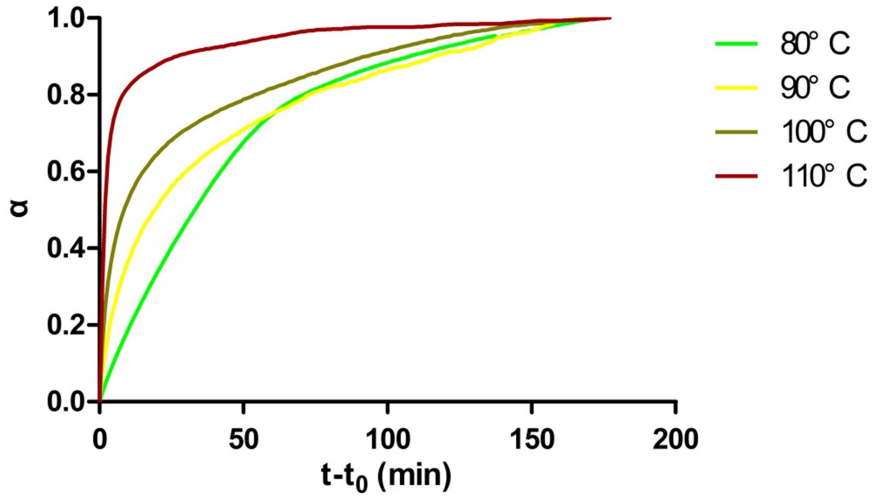

Figure S19. Conversion (α) versus time ($t-t_0$) plots. **Related to Figure 3.** t_0 is the time correction that accounts for the induction period, including the time required to heat the sample to the targeted temperature.

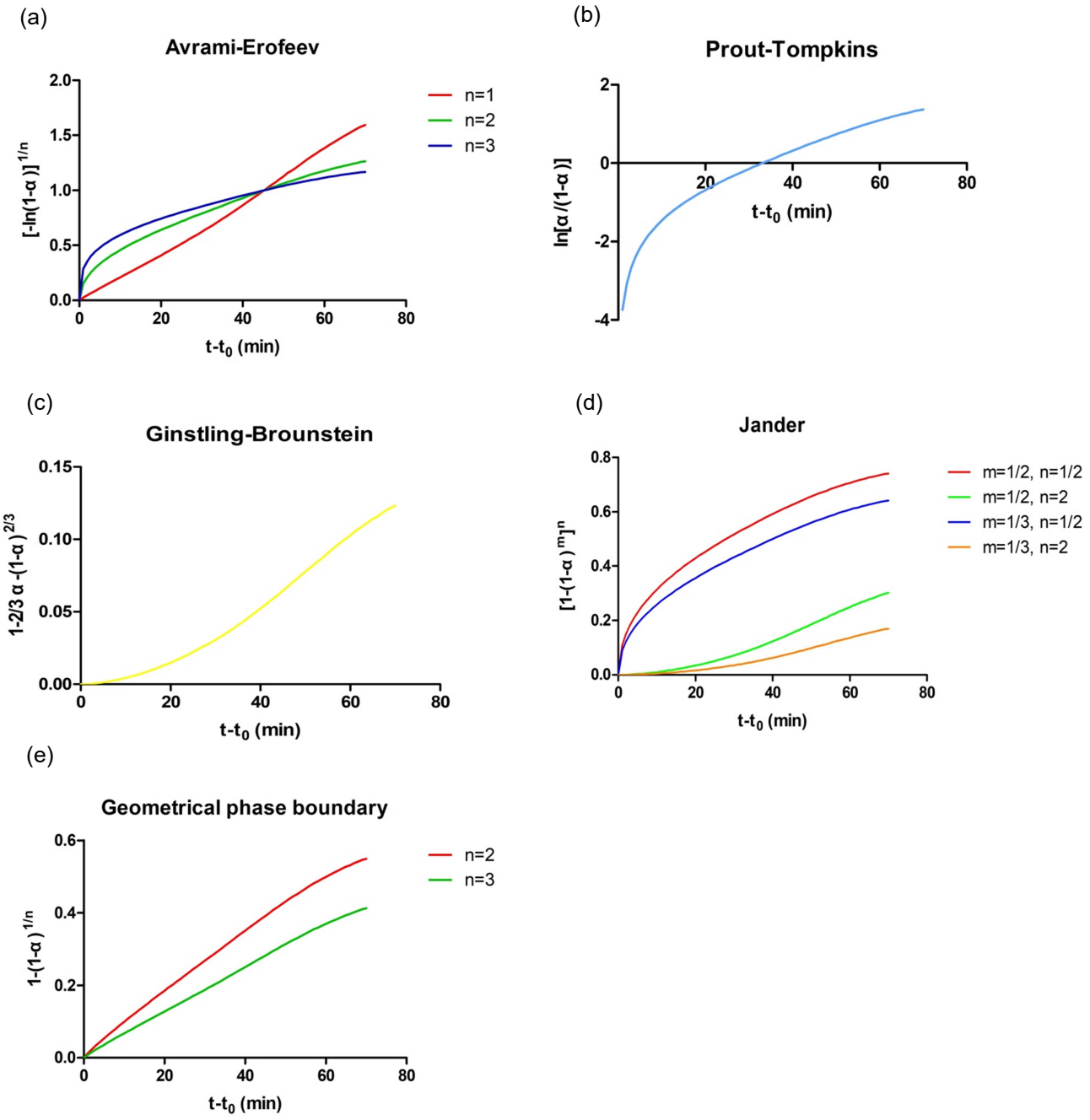

Figure S20. Fitting of the kinetic data to different solid-state kinetic models (showed at 80°C). Related to Figure 3. (a) Avrami-Erofeev model. (b) Prout-Tompkins model. (c) Ginstling-Brounstein model. (d) Jander model. (e) geometrical phase boundary model.

(a)

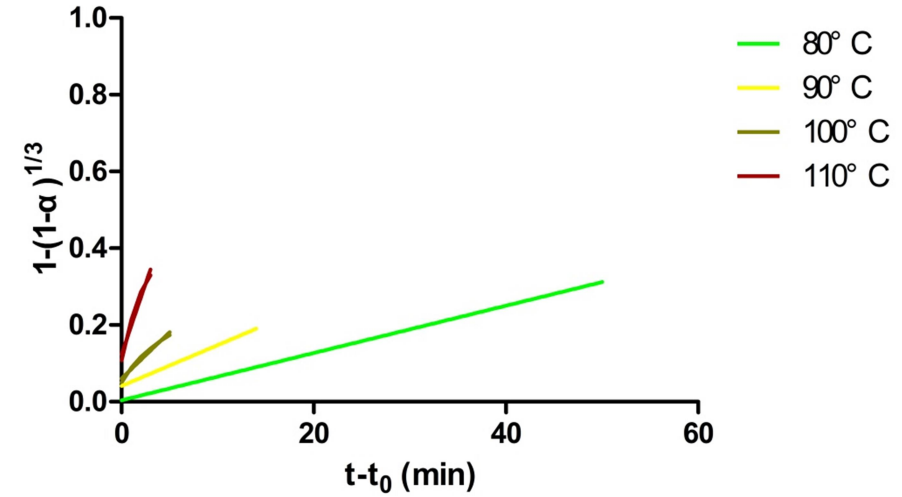

(b)

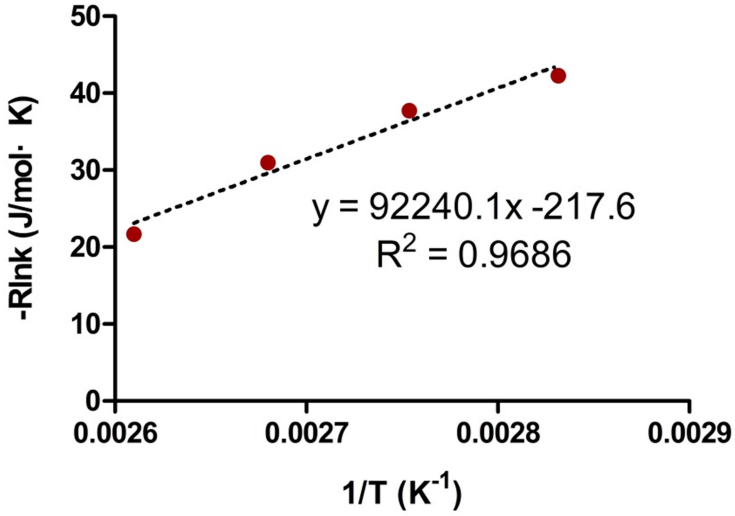

Figure S21. Physicochemical modeling of FuBIG carbonate salt heat release. Related to Figure 3. (a) Fitting of the kinetic data to geometrical phase boundary model. 80°C: y = 0.0062x + 0.0039, R^2 = 0.9998; 90°C: y = 0.0107x + 0.0411, R^2 = 0.9775; 100°C: y = 0.0241x + 0.0608, R^2 = 0.9743; 110°C: y = 0.0736x +0.1240, R^2 = 0.9652. (b) Activation barrier was obtained from Arrhenius analysis of the rate constants (k) under different temperatures.

(a)

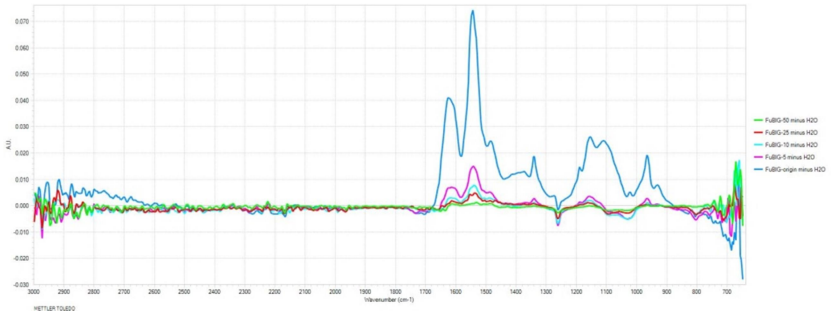

(b)

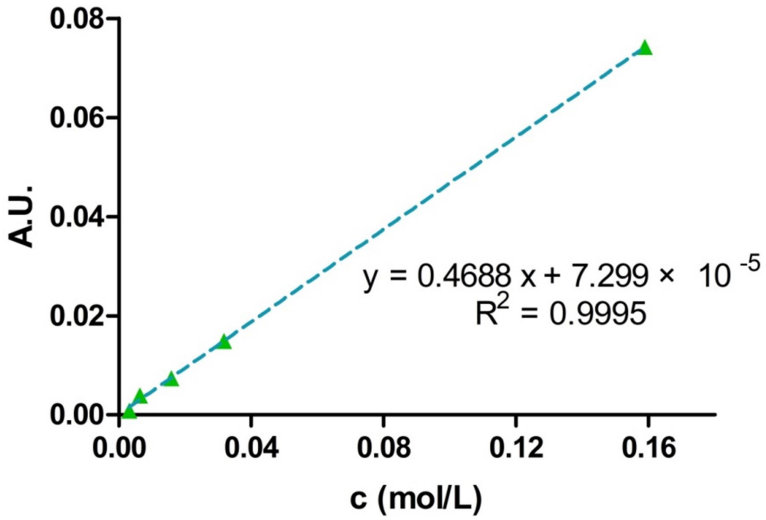

Figure S22. The mathematical relationship between concentration and absorption unit of FuBIG water solution. Related to Figure 3. (a) Absorption of different concentrations of FuBIG in ReactIR. (b) Standard absorption curve of FuBIG concentrate and absorption unit in ReactIR.

(a)

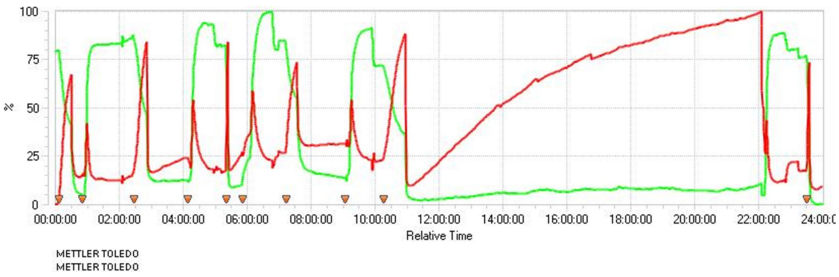

(b)

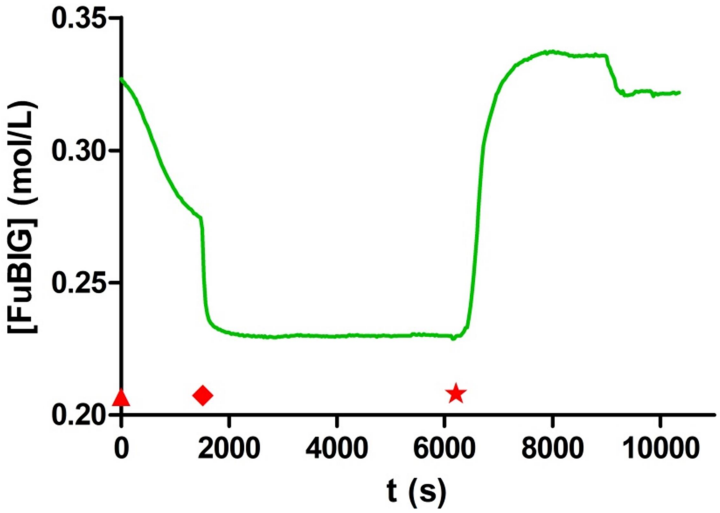

Figure S23. The process of CO_2 absorption-release cycle monitored by React IR. Related to Figure 3. (a) The total process of CO_2 absorption-release of FuBIG. (b) The kinetic profiles of CO_2 absorption were picked between 2:26:55 and 2:48:55. Tiangle: representing the time point for the adding of CO_2 into the solvent. Rhombus: representing the time point for complete conversion of FuBIG to $FuBIGH_2(CO_3)(H_2O)_4$. Five-pointed star: representing the time point for heating.

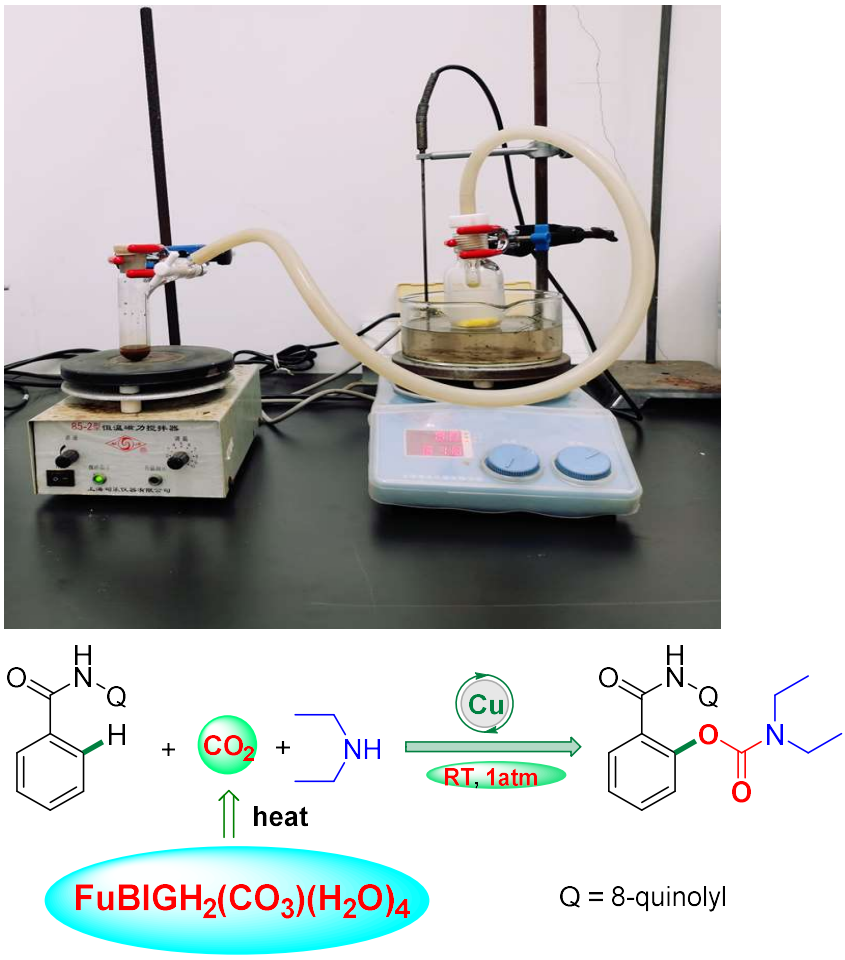

Figure S24. Synthetic utility of CO_2 captured by FuBIG in the copper-catalyzed C−H carbamoyloxylation reaction. Related to Figure 3. CO_2 released from $FuBIGH_2(CO_3)(H_2O)_4$ can be utilized in our previous published transformations. (*Org. Lett. 2019, 21, 2013−2018.*)

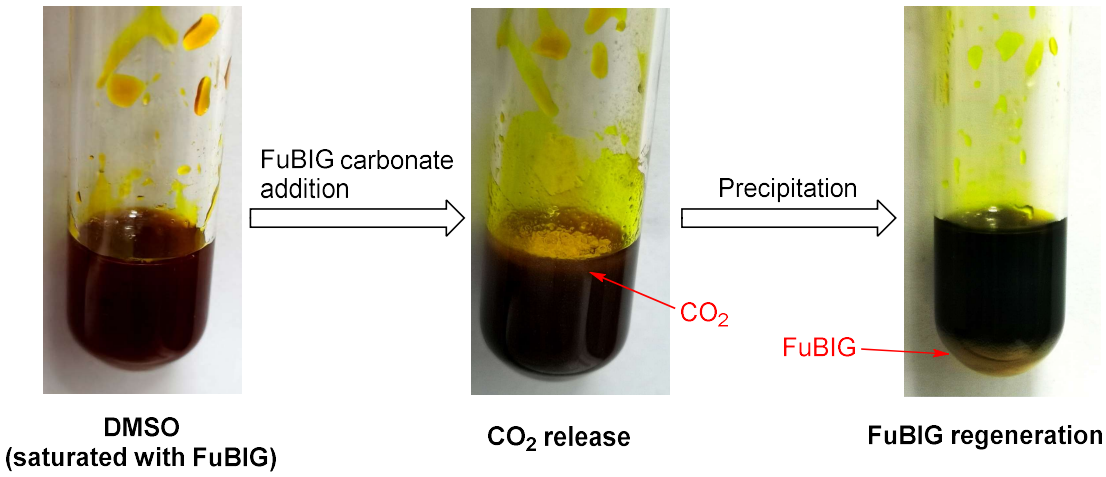

Figure S25. Practical process of FuBIG regeneration with DMSO. Related to Figure 4.

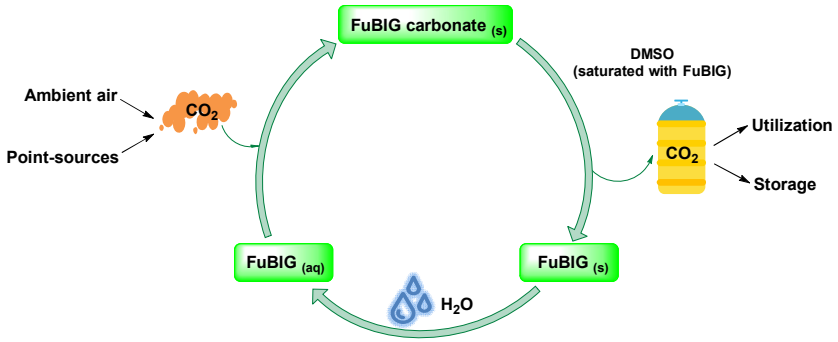

Figure S26. A low-energy protocol for CO_2 capture/release and sorbent regeneration with minimum DMSO consumption. Related to Figure 4. DMSO solution saturated with FuBIG could still promote the release of CO2 from FuBIG carbonate, and lead to the regeneration of FuBIG.

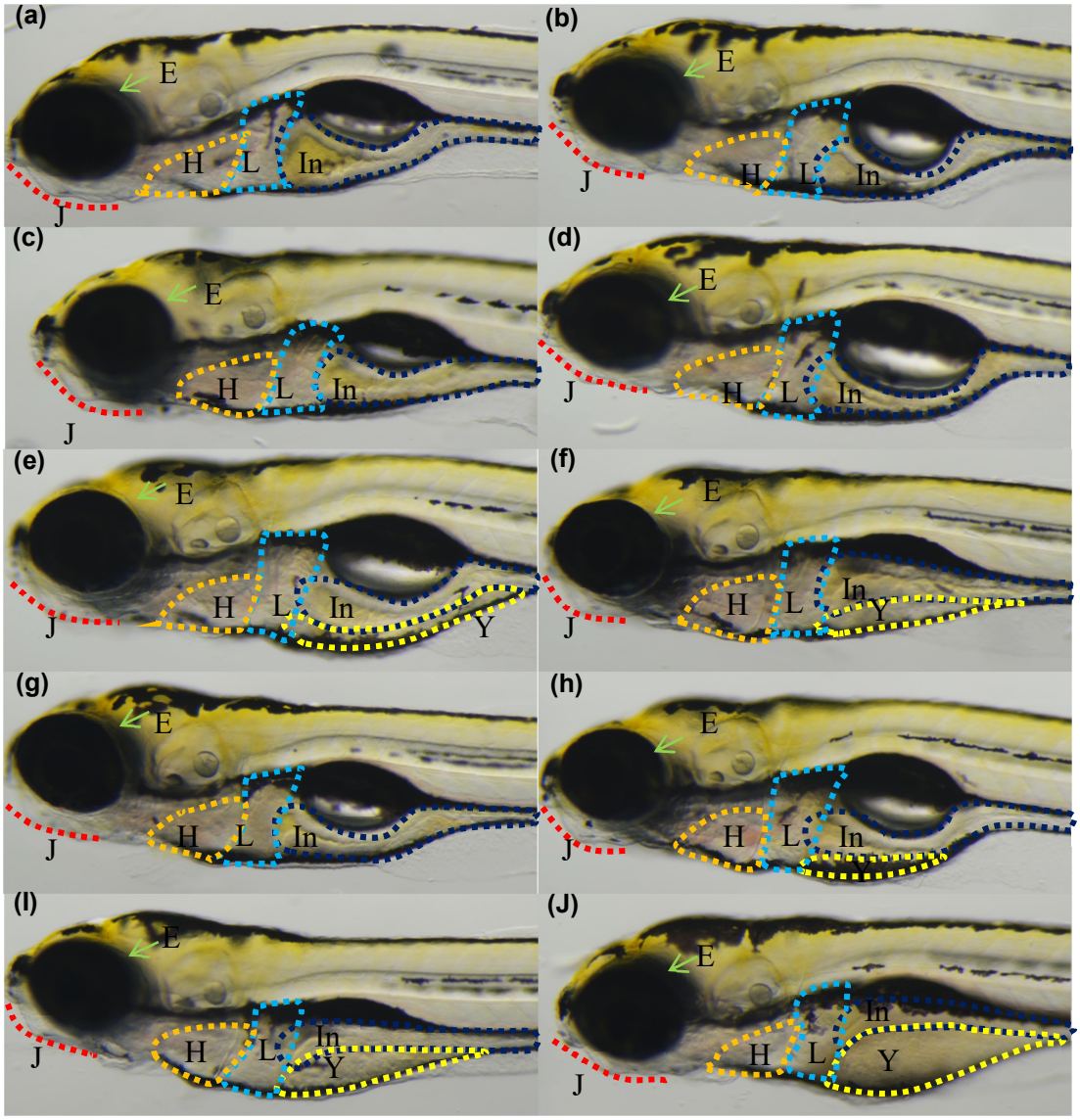

Figure S27. Toxicity of FuBIG and PyBIG in zebrafish testing. Related to Figure 5. (a) Untreated normal control. (b) Zebrafish were treated with 1% DMSO as solvent control. (c) FuBIG 1/9 MNLC. (d) FuBIG 1/3 MNLC. (e) FuBIG MNLC. (f) FuBIG LC_{10}. (g) PyBIG 1/9 MNLC. (h) PyBIG 1/3 MNLC. (I) PyBIG MNLC. (J) PyBIG LC_{10}. H = heart, J = Jaw, In = Intestinal tract, L = Liver, E = eye, Y = Yolk Sac.

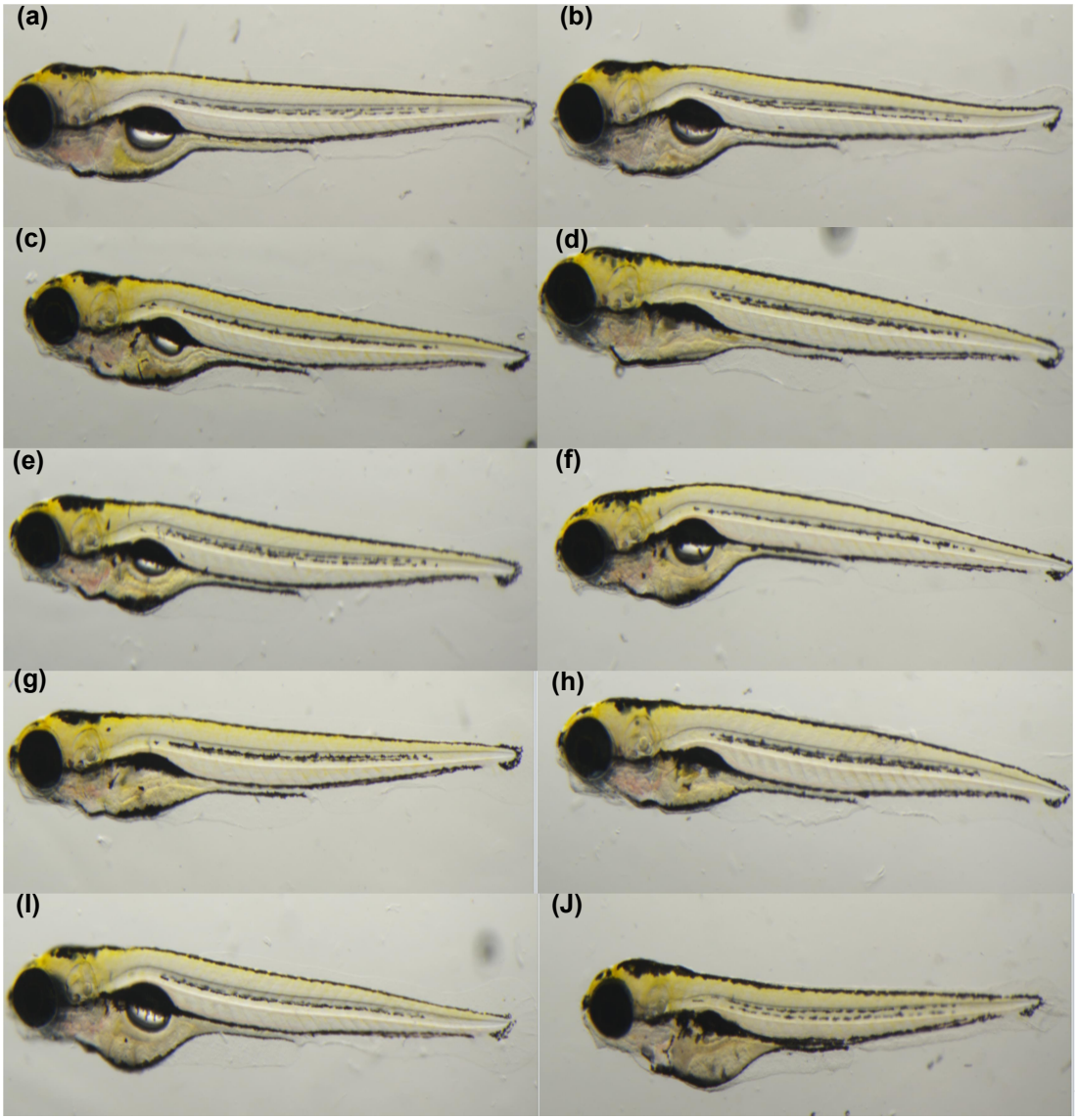

Figure S28. Toxicity of FuBIG and PyBIG in zebrafish embryo testing. Related to Figure 5. (a) Untreated normal control. (b) Zebrafish embryos were treated with 1% DMSO as solvent control. (c) FuBIG 1/9 MNLC. (d) FuBIG 1/3 MNLC. (e) FuBIG MNLC. (f) FuBIG LC_{10}. (g) PyBIG 1/9 MNLC. (h) PyBIG 1/3 MNLC. (I) PyBIG MNLC. (J) PyBIG LC_{10}.

Supplemental Tables

Table S1. Elemental analysis of $FuBIGH_2(CO_3)(H_2O)_4$. Related to Figure 2.

	C [%]	H [%]	N [%]	C/N	C/H
measured	28.50	5.58	29.06	0.9809	5.1096
theoretical	29.19	5.99	30.26	0.9646	4.8731

Table S2. Crystal test parameters of $FuBIGH_2(CO_3)(H_2O)_4$. Related to Figure 2.

Chemical Formula	$C_9H_{22}N_8O_8$
Formula Weight	370.34
Crystal Size (Mm^3)	0.5×0.3×0.2
Crystal System	triclinic
Space Group	P-1
a (Å)	11.1919 (4)
b (Å)	12.7930 (5)
c (Å)	14.1784 (4)
α (deg)	97.547 (3)
β (deg)	111.174 (3)
γ (deg)	112.709 (4)
volume ($Å^3$)	1657.46 (11)
Z	4
density (g/cm^3)	1.484
2θ range	7.044–134.138
F (000)	787.0
index ranges	-13 ≤ h ≤ 13 -15 ≤ k ≤ 15 -11 ≤ l ≤ 16
no. of reflns	11953
no. of unique reflns	5860
no. of params	501
R_{all}, R_{obs}	0.0352, 0.0336
$wR_{2,all}$, $wR_{2,obs}$	0.0892, 0.0880
goodness-of-fit on F^2	1.054

$R_1 = \Sigma||F_o| - |F_c||/\Sigma|F_o|$, $wR^2=[\Sigma[w(F_o^2 - F_c^2)^2] /\Sigma w(F_o^2)^2]^{1/2}$,

$w=1/[\sigma^2(F_o)^2 + (aP^2) + bP]$, where $P=[(F_o^2) + 2F_c^2]/3$.

Table S3. Absorption data for $FuBIGH_2Cl_2$ in different concentrations. Related to Table 1.

Concentration (mol/L)	Absorption
0.00001346	0.1276
0.00002690	0.3067
0.00003365	0.4016
0.00006730	0.9116
0.0001346	1.8974

Table S4. Solubility data for FuBIG at 15-35°C. Related to Table 1.

T (°C)	Solubility (mol/L)
15	0.2277
20	0.2739
25	0.4029
30	0.5953
35	0.8192

Table S5. pH data of saturated solution of $FuBIGH_2(CO_3)(H_2O)_4$ at 15-35°C. Relate to Table 1.

T (°C)	pH
15	8.82
20	8.68
25	8.48
30	8.31
35	8.17

Table S6. Solubility data and calculated value for $FuBIGH_2(CO_3)(H_2O)_4$ at 15-35°C. Relate to Table 1.

T (°C)	Solubility (mol/L)	K_{sp} ($\times 10^{-8}$)
15	0.003899	1.446
20	0.007068	4.042
25	0.009344	6.128
30	0.01318	10.55
35	0.02713	27.92

Table S7. pK_a data for FuBIG at 15-35°C. Relate to Table 1.

T (°C)	pK_{a1}	pK_{a2}
15	7.79	8.90
20	7.68	8.82
25	7.57	8.71
30	7.49	8.66
35	7.31	8.59

Table S8. Absorption data for different concentrations FuBIG in ReactIR. Related to Figure 3.

Concentration (mol/L)	Absorption
0.1589	0.07423
0.03178	0.01490
0.01589	0.007342
0.006356	0.003933
0.003178	0.00082

Table S9. Absorption intensity data monitored at 1533 cm^{-1} (N—H) using React IR when FuBIG carbonate salt being added into DMSO and H_2O respectively. Relate to Figure 4.

Time	A.U. at 1533cm^{-1} in DMSO	A.U. at 1533cm^{-1} in H_2O
00:00:12	0.015584	0.025983
00:00:27	0.015662	0.026056
00:00:42	0.015882	0.025833
00:00:57	0.015789	0.025448
00:01:11	0.015807	0.025254
00:01:27	0.015575	0.025444
00:01:42	0.016172	0.025258
00:01:56	0.015863	0.025088
00:02:11	0.015899	0.025232
00:02:27	0.015468	0.024927
00:02:42	0.015371	0.02474
00:02:57	0.015817	0.02494
00:03:12	0.015371	0.024817
00:03:27	0.01594	0.024991
00:03:42	0.015832	0.024574
00:03:57	0.015571	0.024649
00:04:12	0.016137	0.024753
00:04:26	0.015312	0.024912
00:04:42	0.015361	0.024799
00:04:57	0.015571	0.02493
00:05:12	0.01539	0.024532
00:05:27	0.015058	0.025246
00:05:41	0.015251	0.024929
00:05:57	0.015309	0.024906
00:06:11	0.015094	0.025181
00:06:27	0.015784	0.025324
00:06:41	0.01527	0.025004
00:06:57	0.015581	0.024744
00:07:12	0.015252	0.025361
00:07:27	0.015331	0.023964
00:07:41	0.015134	0.022766
00:07:57	0.021827	0.022361
00:08:12	0.053243	0.021889
00:08:27	0.062639	0.022015
00:08:42	0.065978	0.02145
00:08:56	0.068484	0.021327
00:09:12	0.069669	0.021291
00:09:27	0.07039	0.020931
00:09:42	0.070876	0.020613
00:09:56	0.071583	0.02072

00:10:12	0.072118	0.020691
00:10:27	0.072285	0.020332
00:10:41	0.072672	0.02057
00:10:56	0.072637	0.020668
00:11:12	0.072977	0.020292
00:11:27	0.072714	0.020487
00:11:42	0.072604	0.020336
00:11:57	0.072801	0.020162
00:12:11	0.072886	0.020259
00:12:27	0.073042	0.020169
00:12:41	0.07315	0.019988
00:12:57	0.072603	0.019994
00:13:11	0.073017	0.020357
00:13:27	0.07296	0.019976
00:13:42	0.072799	0.020263
00:13:57	0.073242	0.020133
00:14:12	0.073223	0.020115
00:14:27	0.073186	0.019913
00:14:42	0.073206	0.020044
00:14:57	0.073004	0.019948
00:15:11	0.073203	0.019992
00:15:26	0.073339	0.019996
00:15:42	0.07338	0.019932
00:15:57	0.07317	0.019884
00:16:12	0.07324	0.020251
00:16:27	0.073177	0.019679
00:16:42	0.073341	0.019492
00:16:57	0.073435	0.019708
00:17:11	0.073564	0.019867
00:17:26	0.073634	0.020031
00:17:42	0.073688	0.01999
00:17:57	0.073644	0.019939
00:18:12	0.073695	0.019911
00:18:27	0.073571	0.019986
00:18:41	0.073489	0.019676
00:18:57	0.073555	0.019782
00:19:12	0.073759	0.019742
00:19:27	0.073833	0.019545
00:19:41	0.07413	0.019581
00:19:57	0.073995	0.019713
00:20:12	0.073727	0.019597
00:20:27	0.073561	0.019759
00:20:42	0.073851	0.01975
00:20:56	0.073646	0.019978

00:21:12	0.073997	0.019833
00:21:27	0.073841	0.019925
00:21:41	0.074038	0.019842
00:21:56	0.073841	0.020232
00:22:12	0.074188	0.019747
00:22:26	0.073814	0.020204
00:22:41	0.074055	0.019937
00:22:56	0.073699	0.019965
00:23:12	0.073961	0.019619
00:23:27	0.074076	0.019829
00:23:42	0.073911	0.019745
00:23:56	0.073793	0.019707
00:24:11	0.073845	0.019662
00:24:27	0.073832	0.019742
00:24:42	0.074056	0.019888
00:24:57	0.074118	0.019721

Table S10. Acute toxicity experiment of zebrafish treated with FuBIG and PyBIG. Related to Figure 5.

	Concentration (μM)	Death number	Mortality (%)
Normal	-	0	0
1 % DMSO	-	0	0
FuBIG	4.2	0	0
	21.2	0	0
	42.4	0	0
	75.8	21	70.0
	79.7	23	76.7
	127.1	30	100
	169.5	30	100
PyBIG	3.4	0	0
	17.1	0	0
	30.8	13	43.3
	32.5	16	53.3
	34.2	20	66.7
	68.5	30	100
	102.7	30	100
	137.0	30	100

Table S11. Embryo toxicity experiment of zebrafish embryos treated with FuBIG and PyBIG. Related to Figure 5.

	Concentration (μM)	Death number	Mortality (%)
Normal	-	0	0
1 % DMSO	-	0	0
FuBIG	21.2	0	0
	42.4	0	0
	84.7	10	33.3
	127.1	19	63.3
	169.5	30	100
	211.9	30	100
PyBIG	17.1	0	0
	34.2	8	26.7
	68.5	29	96.7
	102.7	30	100
	137.0	30	100
	171.2	30	100

References

Becke, A.D. (1993). Density-functional thermochemistry. III. The role of exact exchange. J. Chem. Phys. *98*, 5648–5652.

Chakraborty, S., Lagaditis, P.O., Förster, M., Bielinski, E.A., Hazari, N., Holthausen, M.C., Jones, W.D. and Schneider, S. (2014). Well-defined iron catalysts for the acceptorless reversible dehydrogenation-hydrogenation of alcohols and ketones. ACS Catal. *4*, 3994–4003.

Hohenberg, P. and Kohn, W. (1964). Inhomogeneous electron gas. Physical Review *136*, B864–B871.

Frisch, M.J., Trucks, G.W., Schlegel, H.B., Scuseria, G.E., Robb, M.A., Cheeseman, J.R., Scalmani, G., Barone. V., Mennucci, B., Petersson, G.A., et al. (2013). Gaussian 09, Revision D.01 (Gaussian, Inc., Wallingford CT).

Grimme, S., Antony, J., Ehrlich, S. and Krieg, H. (2010). A consistent and accurate *ab initio* parametrization of density functional dispersion correction (DFT-D) for the 94 elements H-Pu. J. Chem. Phys. *132*, 154104.

He, J.H., Guo, S.Y., Zhu, F., Zhu, J.J., Chen, Y.X., Huang, C.J., Gao, J.M., Dong, Q.X., Xuan, Y.X. and Li, C.Q. (2013). A zebrafish phenotypic assay for assessing drug-induced hepatotoxicity. J. Pharmacol. Toxicol. Methods. *67*, 25–32.

Huang, Z. (2010). Introduction of electrolyte solution theory (Science Press).

Kimmel, C.B., Ballard, W.W., Kimmel, S.R., Ullmann, B. and Schilling, T.F. (1995). Stages of embryonic development of the zebrafish. Developmental dynamics *203*, 253–310.

Kohn, W. and Sham, L.J. (1965). Self-consistent equations including exchange and correlation effects. Physical Review *140*, A1133–A1138.

Lee, C., Yang, W. and Parr, R.G. (1988). Development of the Colle-Salvetti correlation-energy formula into a functional of the electron density. Phys Rev B Condens Matter *37*, 785–789.

Legault, C.Y. (2009). CYLview, 1.0b (Université de Sherbrooke). http://www.cylview.org.

Luo, X., Song, X., Xiong, W., Li, J., Li, M., Zhu, Z., Wei, S., Chan, A.S.C. and Zou, Y. (2019). Copper-catalyzed C–H carbamoyloxylation of aryl carboxamides with CO_2 and amines at ambient conditions. Org. Lett. *21*, 2013–2018.

Marenich, A.V., Cramer, C.J. and Truhlar, D.G. (2009). Universal solvation model based on solute electron density and on a continuum model of the solvent defined by the bulk dielectric constant and atomic surface tensions. J. Phys. Chem. B. *113*, 6378–6396.

Peiper, J.C. and Pitzer, K.S. (1982). Thermodynamics of aqueous carbonate solutions including mixtures of sodium carbonate, bicarbonate, and chloride. J. Chem. Thermodynamics. *14*, 613–638.

Petersson, G.A. and Al-Laham, M.A. (1991). A complete basis set model chemistry. II. Open-shell systems and the total energies of the first-row atoms. J. Chem. Phys. *94*, 6081–6090.

Petersson, G.A., Bennett, A., Tensfeldt, T.G., Al-Laham, M.A., Shirley, W.A. and Mantzaris, J. (1988). A complete basis set model chemistry. I. The total energies of closed-shell atoms and hydrides of the first-row elements. J. Chem. Phys. *89*, 2193–2218.

Stefánsson, A., Bénézeth, P. and Schott, J. (2013). Carbonic acid ionization and the stability of sodium bicarbonate and carbonate ion pairs to 200 C – A potentiometric and spectrophotometric study. Geochimica. et. Cosmochimica. Acta. *120*, 600–611.

Vosko, S.H., Wilk, L. and Nusair, M. (1980). Accurate spin-dependent electron liquid correlation energies for local spin density calculations: a critical analysis. Canadian Journal of Physics *58*, 1200–1211.

Westerfield M. (1995). The Zebrafish Book. A Guide for the Laboratory Use of Zebrafish (Danio rerio) (University of Oregon Press).

Zhu, J.J., Xu, Y.Q., He, J.H., Yu, H.P., Huang, C.J., Gao, J.M., Dong, Q.X., Xuan, Y.X. and Li, C.Q. (2014). Human cardiotoxic drugs delivered by soaking and microinjection induce cardiovascular toxicity in zebrafish. J. Appl. Toxicol. *34*, 139–148.